regarded as a major PAD in the CNS that contributes to the pathogenesis of neurodegeneration (3, 17, 18). Overexpression and activation of PAD2 result in excessive citrullination in reactive astrocytes of the hippocampal region in AD and scrapie-infected mice (1, 3). Peptidylarginine deiminase 2–mediated MBP citrullination suggests a role in the pathogenesis of MS. Myelin basic protein citrullination affects the interaction of the molecule with phospholipids, changes its 3-dimensional structure and increases susceptibility to proteases such as cathepsin D (4). In addition, PAD2 transgenic mice show activation of astrocytes and microglia and accumulation of citrullinated proteins, suggesting a relationship between the pathogenesis of MS and MS-like diseases (19).

Thus far, the localization patterns of PAD2 and citrullinated proteins in neurodegenerative diseases, particularly prion diseases, have been incompletely characterized. Prion diseases are fatal neurodegenerative diseases that can have a genetic, infectious or unknown (termed *sporadic*), basis. Prion diseases are characterized by neuronal loss, spongiform degeneration, reactive gliosis, and accumulation of proteinase K–resistant misfolded prion proteins (PrP^{Sc}) in the brain (20, 21). In prion disease–affected brains, there are dramatic changes in brain proteins such as alteration of expression levels and inherent functions and posttranslational modifications of various proteins including PrP (22–26). We previously showed that the enzyme activity and protein expression of PAD2 as well as the citrullinated protein level correlated with the progression of this disease and reached a maximum level at the end stage of scrapie infection (1). To understand the change and correlation of expression and localization patterns between PAD2 and citrullinated proteins in normal and disease status, we performed subcellular fractionation and electron microscopic analysis of the brains of normal and scrapie-infected mice as a model of prion diseases. We report the nuclear localization of PAD2 and the detailed subcellular localization of PAD2 and citrullinated proteins in scrapie-infected versus uninfected mouse brains.

MATERIALS AND METHODS

Reagents

All chemicals and reagents used were purchased from Sigma-Aldrich (St Louis, MO) unless stated otherwise.

Scrapie Strain and Animals

The original stock of ME7 scrapie strain was kindly provided by Dr Alan Dickinson of Agriculture and Food Research Council and Medical Research Council Institute (Edinburgh, UK). This scrapie strain was maintained by serial intracerebral passage of brain homogenate from terminally affected mice. C57BL/6J mice (Central Laboratory Animal, Inc, Seoul, Republic of Korea), aged 4 to 6 weeks, were inoculated intracerebrally with 30 μL of 1% (wt/vol) brain homogenate in 0.01 mol/L phosphate-buffered saline (PBS) prepared from ME7-injected C57BL/6J mice or from control mice that had been injected with normal brain homogenate. Mice were killed at 150 ± 10 days after inoculation with ME7 scrapie strain, a time when clinical manifestations of disease were evident. Thirty-six C57BL/6J mice were used in the study. Eighteen mice (3 separate experiments performed in triplicate: control, n = 9; scrapie-infected, n = 9) were used for subcellular fractionation, 12 mice (2 separate experiments performed in triplicate: control, n = 6; scrapie-infected, n = 6) were used for nuclear fractionation, and 6 mice (control, n = 3; scrapie-infected, n = 3) were fixed for electron microscopic analysis. Animal experiments and research protocols were approved by the Institutional Animal Care and Use Committee (approval code HMC2009-1-0714) of Hallym University.

Cell Culture and Transfection

H4 human neuroglioma cells were maintained in Dulbecco modified Eagle medium containing 4 mmol/L L-glutamine, 4500 mg/L D-glucose, and sodium pyruvate (HyClone Laboratories, Logan, UT) supplemented with 10% fetal bovine serum (HyClone Laboratories) and 100 U/mL penicillin, 100 μg/mL streptomycin (GIBCO, Grand Island, NY) at 37°C in a 5% CO_2 atmosphere. H4 cells stably expressing full-length human PAD2 (1–665 amino acids) were generated by transfection with a pcDNA3.1/Zeo(+)-PAD2 (Invitrogen, Carlsbad, CA) construct using SuperFect (QIAGEN GmbH, Hilden, Germany), followed by selection and maintenance in the presence of 200 μg/mL Zeocin (Invitrogen).

Subcellular Fractionation

Mouse brain tissues were homogenized with 10 volumes of isotonic homogenization buffer (10 mmol/L Tris-HCl, pH 7.4, 250 mmol/L sucrose, 10 mmol/L KCl, 1.5 mmol/L $MgCl_2$, 1 mmol/L ethylenediaminetetraacetic acid [EDTA], 1 mmol/L sodium vanadate). After 20 up-and-down strokes in a Dounce homogenizer, the crude homogenates were subjected to subcellular fractionation by differential centrifugation to give mitochondrial, microsomal, and cytosolic fractions. Briefly, nuclei and unbroken cells were removed by centrifugation at 800 × *g* for 5 minutes at 4°C. The postnuclear supernatant was then sequentially centrifuged at 13,500 × *g* for 10 minutes to get a crude mitochondrial pellet. The remaining supernatant was further centrifuged at 105,000 × *g* for 1 hour at 4°C to obtain a microsomal pellet and the remaining supernatant (cytosolic fraction). All pellets were rinsed twice with isotonic buffer and resuspended with lysis buffer containing 50 mmol/L Tris-HCl, pH 7.4, 150 mmol/L NaCl, 1 mmol/L EDTA, 1 mmol/L sodium vanadate (EMD Chemicals, Darmstadt, Germany), 1% Triton X-100, 1% Nonidet P-40, and 0.25% sodium deoxycholic acid and protease inhibitors (Roche Diagnostics, Indianapolis, IN) and then homogenized by sonication. For nuclear fractions, fresh brain tissues were homogenized in fractionation buffer A (10 mmol/L Tris-HCl, pH 8.0 buffer containing 0.32 mol/L sucrose, 2 mmol/L magnesium acetate [AMRESCO, Solon, OH], 0.1 mmol/L EDTA, 1 mmol/L dithiothreitol [DTT; Bio-Rad, Hercules, CA], 0.5% Nonidet P-40, and protease inhibitors). Brain homogenates were then centrifuged at 3,000 × *g* for 10 minutes at 4°C. Nuclear-containing pellets were suspended with

fractionation buffer A and then mixed with fractionation buffer B (10 mmol/L Tris-HCl, pH 8.0 buffer containing 2 mol/L sucrose, 5 mmol/L magnesium acetate, 0.1 mmol/L EDTA, and 1 mmol/L DTT) in the ratio of 1:1. The nuclear homogenates were layered onto fractionation buffer B and then centrifuged at 30,000 × *g* for 1 hour at 4°C. Nuclear pellets from control and scrapie-infected brains were dissolved in lysis buffer as described above. Fractionation efficiency was evaluated by Western blotting with rabbit polyclonal anti-Cu,Zn-superoxide dismutase (anti-Cu,Zn SOD, 1:1000; Millipore, Bedford, MA), rabbit polyclonal anti-histone H3 (1:5000; Abcam, Cambridge, MA), and anti-enolase 1 (1:5000; AbFrontier, Seoul, Republic of Korea) diluted in PBS containing 1% Tween 20 (PBST). For the cultured cells, cytoplasmic and nuclear protein fractions were extracted by using a ProteoJet cytoplasmic and nuclear protein extraction kit (Fermentas, Glen Burnie, MD).

Western Blot Analysis

The protein concentration of homogenates was determined with a BCA protein assay kit (Pierce, Rockford, IL). Citrullinated proteins were detected by Western blot analysis as previously described (27). Briefly, equal amounts of protein (50 μg/lane) were subjected to 12% SDS-PAGE and transferred to polyvinylidene diflouride (PVDF) membrane (Millipore) using an electrotransfer system (Bio-Rad). For detection of citrullinated proteins, citrulline residues on the PVDF membrane were chemically modified by overnight incubation at 37°C in modification reagent (1 vol of buffer 1: a mixture of 1% diacetyl monoxime/0.5% antipyrine/1 mol/L acetic acid; and 2 vol of buffer 2: a mixture of 85% H_3PO_4/98% H_2SO_4/H_2O [20/25/55] containing 0.1% $FeCl_3 \cdot 6H_2O$). The membrane was then blocked with 4% nonfat dry milk in PBST (8 mmol/L Na_2HPO_4, 2 mmol/L KH_2PO_4, 138 mmol/L NaCl, 2.7 mmol/L KCl, pH 7.4, 0.1% Tween 20) for 1 hour at room temperature (RT), then probed with a rabbit polyclonal anti-modified citrulline antibody at 1:1000 (Upstate, Lake Placid, NY) in PBST overnight at 4°C. For Western blot analysis of other target proteins, mouse monoclonal anti-PAD2 antibody (1:5000) (28), mouse monoclonal anti–neuron-specific enolase (NSE, 1:10,000; AbFrontier), rabbit polyclonal anticalnexin (1:2000; Santa Cruz Biotechnology, Santa Cruz, CA), goat polyclonal anti-cytochrome *c* (1:1000; Santa Cruz Biotechnology), and rabbit polyclonal anti-PAD4 (1:500; Abgent, San Diego, CA) were directly probed in PBS with or without 4% nonfat dry milk. Target antibody-attached PVDF membranes were then incubated with the appropriate secondary antibody conjugated to horseradish peroxidase. Immunoreactive signals were detected on x-ray film (Agfa, Mortsel, Belgium) by chemiluminescent substrate as described by the manufacturer (Amersham Biosciences, Piscataway, NJ).

PAD Enzyme Activity

Peptidylarginine deiminase 2 activity was determined as previously described (29). Briefly, subcellular fractionated proteins (50 μg) were incubated with reaction mixture containing 100 mmol/L Tris-HCl, pH 7.5, 10 mmol/L $CaCl_2$, 5 mmol/L DTT, with or without 10 mmol/L benzoyl-L-arginine ethyl ester (BAEE) in a final volume of 100 μL at 50°C for 6 hours. After incubation, the reaction was stopped by adding final 1 mol/L perchloric acid. Samples were cooled on ice for 20 minutes and then centrifuged at 18,000 × *g* for 5 minutes at RT. One hundred microliters of supernatants was mixed with 600 μL of color-developing reagents (1 vol of a mixture of 80 mmol/L diacetyl monoxime and 2 mmol/L thiosemicarbazide in dH_2O, and 3 vol of a mixture of 85% H_3PO_4/98% H_2SO_4/H_2O [30/20/50] containing 0.1% $FeCl_3 \cdot 6H_2O$) and incubated at 95°C for 15 minutes. The samples were cooled to RT, and the absorbance was monitored at 534 nm by ELISA reader (VersaMax; Molecular Devices, Sunnyvale, CA).

Immunogold Electron Microscopy

The animals were killed by perfusion with 2.5% glutaraldehyde and 4% paraformaldehyde buffered with 0.1 mol/L PBS, pH 7.4, under deep anesthesia with 16.5% urethane. The hippocampi were trimmed into small pieces immediately after surgical removal and kept in the same fixative for 2 hours at 4°C. Postfixation was done in 1% OsO_4 buffered with PBS, followed by dehydration through a graded ethanol series and embedding in Epon 812. For ultrastructural analysis, nickel grids with epoxy-embedded ultrathin sections (90 nm) were cut with an RMC MTXL ultramicrotome (Tucson, AZ). Ultrathin sections for etching were immersed in a target retrieval solution (pH 9; DAKO, Glostrup, Denmark) and then incubated for 20 minutes at 90°C. The sections were blocked with 0.5% bovine serum albumin (BSA) in PBS for 20 minutes and then incubated with anti-PAD2 antibody (1:100). For immunolabeling of citrullinated proteins, the sections were incubated for 90 minutes at 37°C in modification reagent for citrulline residue (equal volume of buffers 1 and 2). After modification, sections were blocked with 0.5% BSA in PBS for 20 minutes and then incubated with rabbit polyclonal anti-modified citrulline antibody (1:100) in 0.5% BSA in PBS and 0.5 mol/L NaCl for 1 hour at 60°C. To confirm the specificity of the immunogold procedure, negative controls were treated with either gold-conjugated secondary antibody (goat anti-rabbit IgG, 10 nm) without prior incubation of the section with the primary antibody or nonspecific secondary antibody (goat antimouse IgG). After washing with 0.5% BSA in PBS containing 0.5 mol/L NaCl, 0.1% gelatin, and 0.05% Tween 20, sections were incubated with a goat antirabbit IgG conjugated to 10-nm gold particles or goat antimouse IgG conjugated to 10-nm gold particles (Electron Microscopy Sciences, Hatfield, PA), which was diluted 1:50 in PBS containing 0.5% BSA and 0.5 mol/L NaCl for 1 hour at 60°C. After washing, all sections were treated with PBS containing 0.5% BSA, 0.5 mol/L NaCl, 0.1% gelatin, and 0.05% Tween 20 and then fixed with 2.5% glutaraldehyde in PBS for 10 minutes at RT followed by a final rinse in distilled water. Sections were poststained with uranyl acetate and lead citrate in the usual manner. The sections were examined with a transmission electron microscope (JEM-1011; JEOL Ltd., Tokyo, Japan). To compare the density of gold particles between control and scrapie-infected brains, average numbers of PAD2 gold particles were determined in at least 12 to 25 different astrocytes or neurons; gold particles of citrullinated proteins were determined in at least 13 to 30 different

astrocytes or neurons in the hippocampal sections from 3 different control and scrapie-infected mice. The immunoparticles were counted in subcellular compartments using distinct area parameters: mitochondria, Golgi apparatus, and endoplasmic reticulum (ER) in whole structure; cytoplasm, glial filaments, and nucleus in 0.25 μm^2 squares; and plasma membrane and nuclear membrane in 1-μm lengths of the membranes.

Statistical Analysis

Statistical significance was displayed as mean ± SEM. The probability of statistical differences between control and scrapie-infected groups was determined by a 2-sample *t* test (2-sided) for means. Statistical differences were considered significant at *, $p < 0.05$, **, $p < 0.01$, and ***, $p < 0.001$.

RESULTS

Expression and Localization of PAD2 in Subcellular Fractions of Scrapie-Infected Brains

In previous studies, a prominent increase in PAD2 expression was detected in brains of scrapie-infected mice and of patients with sporadic Creutzfeldt-Jakob disease (1, 2). By Western blot analysis, we found that most PAD2 was localized in the cytosol (Fig. 1A). The content of each fraction was confirmed using the specific markers NSE (a glycolytic enzyme in cytosol), calnexin (integral ER protein) for the microsomal fraction, and cytochrome *c* as a mitochondria-enriched protein. Consistent with our previous result (1), PAD2 expression was significantly increased in each fraction of scrapie-infected brains versus controls (Fig. 1B). To examine the enzymatic activity of PADs from each fraction, the conversion ratio of BAEE was determined (1, 2). Deiminated BAEE was significantly increased in cytosolic, microsomal, and mitochondrial fractions from scrapie-infected brains versus controls (Fig. 1C). As previously reported (1), elevated PAD activity was associated with increased PAD2 expression in scrapie-infected brains. For both scrapie and controls, PAD2 was predominantly expressed and localized in cytosolic fractions with lower levels in membrane fractions containing mitochondria and microsomes.

Accumulation of Citrullinated Proteins in Membrane Fractions of Scrapie-Infected Brains

Recently, we reported that citrullinated proteins were abundantly accumulated in most brain regions in scrapie-infected brains (1). Consistent with our previous results, citrullinated proteins in all fractions of scrapie-infected brains were increased markedly versus controls (Fig. 1D). Interestingly, citrullinated proteins were more abundant in microsomal and mitochondrial fractions compared with cytosolic fraction. In the cytosol, 1 band at approximately 50 kd was predominant, whereas various sizes of citrullinated proteins were seen in membrane fractions. This result demonstrates that the expression and localization level of PAD2 is not directly correlated with hypercitrullination and accumulation of citrullinated proteins.

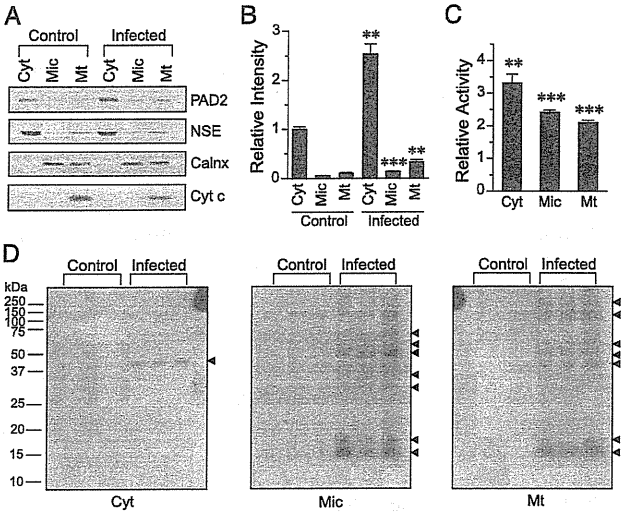

FIGURE 1. Distribution of peptidylarginine deiminase 2 (PAD2) and citrullinated proteins in various subcellular fractions of control and scrapie-infected brain. **(A)** Each fraction of brain homogenates was evaluated by anti-NSE as a cytosolic (Cyt) marker, anticalnexin (Calnx) as a membrane marker, and anti-cytochrome *c* (Cyt *c*) as a mitochondrial (Mt) marker. Peptidylarginine deiminase 2 expression levels were greater in the Cyt versus microsomal (Mic) and Mt fractions under equal loading protein concentrations. Similar results were obtained in at least 3 control and 3 scrapie-infected animals. **(B)** PAD2 expression levels in Cyt, Mic, and Mt fractions of control (n = 3) and scrapie-infected brains (n = 3) measured by scanning densitometry. **(C)** PAD activity was determined using benzoyl-L-arginine ethyl ester (BAEE) as a substrate. Peptidylarginine deiminase activity in Cyt, Mic, and Mt fractions is represented as a ratio of relative units of infected over control fractions (n = 3 each). Significant differences between control and scrapie-infected brains are marked by asterisks (**, $p < 0.01$; ***, $p < 0.001$). **(D)** Using equal amounts of protein in each fraction (40 μg/lane), expression levels of citrullinated proteins were analyzed by Western blotting with an anti-modified citrulline antibody. Each lane shows a separate brain. Arrowheads indicate the bands of hypercitrullinated proteins. Similar results were obtained in 3 separate experimental groups (control and scrapie-infected, n = 3).

Immunogold-Labeled PAD2 in Subcellular Compartments of Hippocampal Astrocytes and Neurons

Immunogold-labeled PAD2 was widely distributed in both astrocytes and neurons, and the immunoparticles were located in various cellular compartments including mitochondrion, ER, Golgi apparatus, and freely in the cytoplasm (Figs. 2, A–D). Distinct mitochondria (Figs. 2E, F), Golgi apparatus (Fig. 2G), and ER structures (Fig. 2H) were observed in astrocytes and neurons. Unique glial filaments were assembled only in astrocytes of scrapie-infected brain

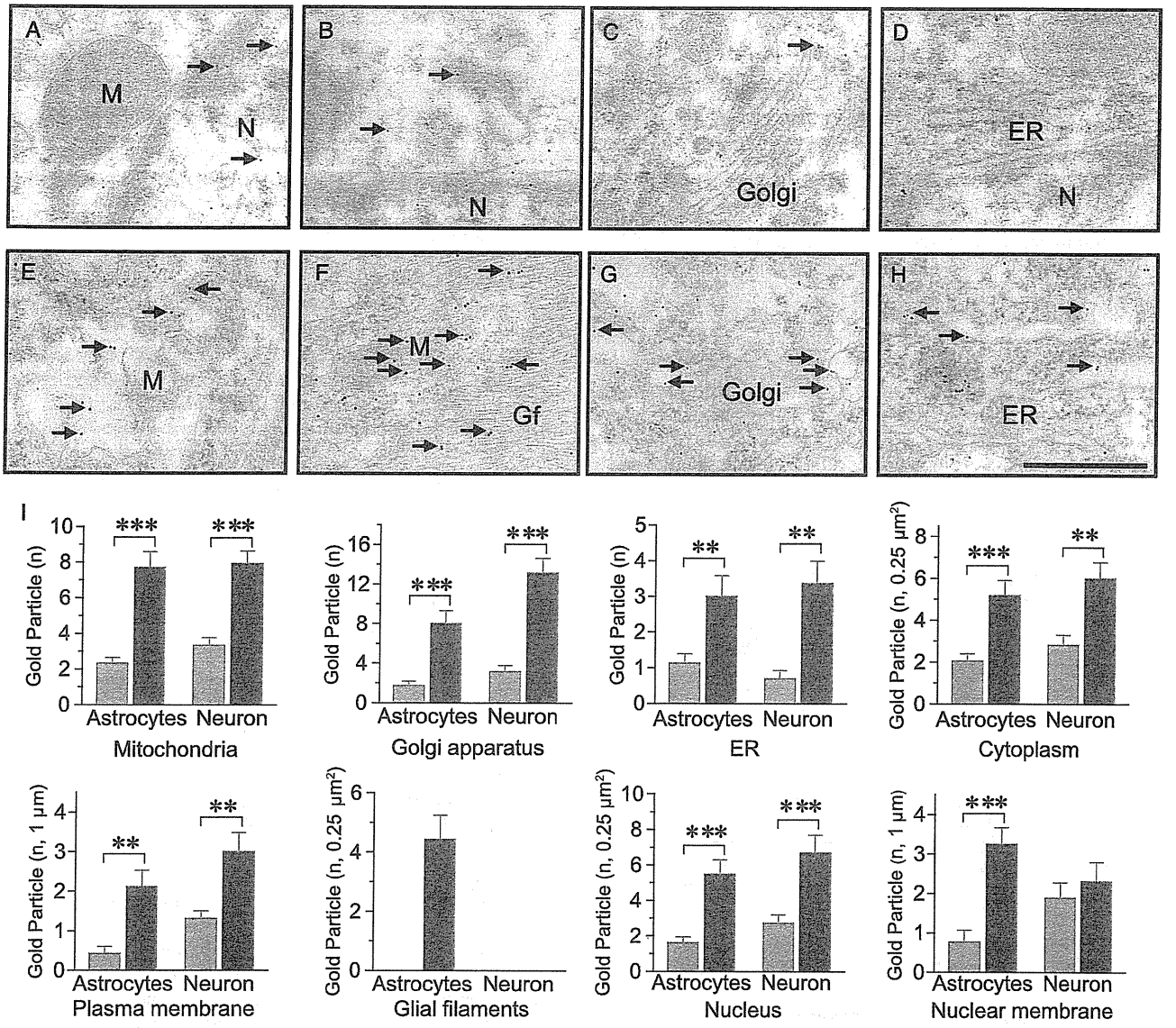

FIGURE 2. Immunogold labeling of peptidylarginine deiminase 2 (PAD2) in hippocampal astrocytes and neurons. **(A–H)** Ten-nanometer immunogold particles (arrows) indicate PAD2 in astrocytes **(A, B, E, F)** and neurons **(C, D, G, H)** of control **(A–D)** and scrapie-infected **(E–H)** brains. ER indicates endoplasmic reticulum; Gf, glial filaments; Golgi, Golgi apparatus; M, mitochondrion; N, nucleus. Scale bars = 500 nm. **(I)** PAD2 immunogold particles were counted in whole mitochondria (n = 27, 26, 23, and 26: respective columns), Golgi apparatus (n = 15, 15, 16, 12), and ER (n = 16, 12, 13, 16). Particles in cytoplasm (n = 20, 17, 17, 15), glial filaments (n = 16), and nuclei (n = 21, 16, 19, 13) were counted in 0.25-μm^2 squares. Particles in plasma membranes (n = 14, 17, 19, 15) and nuclear membranes (n = 17, 16, 18, 13) were counted in 1-μm lengths of membranes. The columns represent the average number of particles at least 12 to 25 different cells in the sections from each sample (control and scrapie-infected, n = 3). Gray columns, control brains; dark columns, scrapie-infected brains. Peptidylarginine deiminase 2 immunogold particles in glial filaments were only labeled in astrocytes of scrapie-infected mice. For control versus scrapie-infected brains: **, $p < 0.01$; ***, $p < 0.001$.

(Fig. 2F). Interestingly, we also found immunoparticles of PAD2 in nuclei. Peptidylarginine deiminase 2 immunogold particles were labeled in most subcellular compartments including mitochondria, glial filaments, ER, Golgi apparatus, and nuclear structure of astrocytes and neurons from scrapie-infected mice. The labeling in controls was significantly lower in all fractions except neuronal nuclear membranes (Fig. 2I).

Nuclear Localization of PAD2 and Citrullination of Nuclear Proteins

We next examined PAD2 expression in nuclear fractions of control and scrapie-infected brains. Surprisingly, the PAD2 expression level in nuclear fractions was not remarkably different from that in cytosolic fractions. As with other fractions, the level was significantly increased in scrapie-infected brains versus controls (Figs. 3A, B). We also confirmed that nuclear localization of PAD2 from nuclear extracts was significantly increased in brains of sporadic Creutzfeldt-Jakob disease cases (data not shown). It has been shown that PAD4 is localized and overexpressed in the nucleus and the myelin fractions in MS and in MS animal models (16, 30). As shown in Figure 3A, immunoblotting of brain cytosol and nuclear fractions yielded very low levels of PAD4, and no difference in expression level between control and scrapie-infected mice was seen. By Western blotting using an anti-modified citrulline antibody, citrullinated proteins were significantly increased in nuclei of scrapie-infected versus control brains (Fig. 3C). To support the finding that PAD2 is localized in nuclei, H4 human neuroblastoma cells stably expressing human PAD2 protein also showed high levels of PAD2 in nuclear fractions (Fig. 3D). These results indicate that PAD2 is localized and overexpressed in the nucleus of scrapie-infected brains.

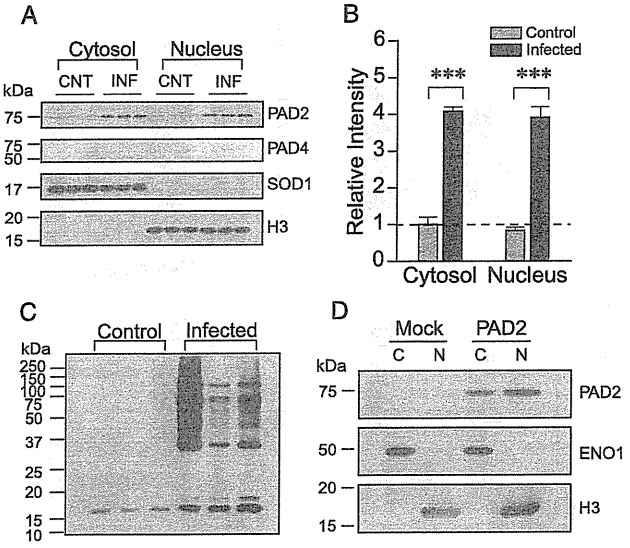

FIGURE 3. Localization of peptidylarginine deiminase 2 (PAD2) in nuclear fractions of control (CNT) and scrapie-infected (INF) brains. **(A)** Nuclear fractions of obtained were evaluated using anti-Cu,Zn-SOD (SOD1) (cytosol) and anti-histone H3 (H3) (nucleus) antibodies. Peptidylarginine deiminase 2 protein was probed with mouse monoclonal anti-PAD2 (2110) antibody. Nuclear PAD4 was probed with an anti-PAD4 (center-specific) antibody. Control and scrapie-infected brains, n = 3. **(B)** Relative intensity of PAD2 in cytosol and nuclear fractions (from **A**) of control and scrapie-infected mice analyzed by scanning densitometry. ***, $p < 0.001$. **(C)** Detection of citrullinated proteins in nuclear fractions of control and scrapie-infected mice. Nuclear proteins (20 μg/lane) were loaded onto 13% SDS-PAGE and then detected by Western blotting using an anti–modified citrulline antibody. **(D)** Nuclear localization of PAD2 an in vitro system. Human PAD2 construct was stably transfected into H4 cell line; cytoplasmic and nuclear fractionation was then performed. α-Enolase (ENO1) was used as a cytoplasmic marker. C indicates cytoplasmic fraction; N, nuclear fraction.

Immunogold-Labeled Citrullinated Proteins in Subcellular Compartments of Hippocampal Astrocytes and Neurons

Similar to the results of PAD2 immunogold labeling, immunogold-labeled citrullinated proteins were associated with astrocyte glial filaments (Fig. 4F) and were observed in mitochondria (Figs. 4A, B, F), Golgi (Figs. 4C, G), ER (Figs. 4D, H), and nuclei (Figs. 4A, E) in hippocampal astrocytes and neurons of control and scrapie-infected brains. Gold particles were not present in serial sections of the negative controls. In nuclear structures, the particles were at a high density in nuclear membrane and perinuclear heterochromatin structures (Fig. 4E), consistent with the Western blot analysis (Fig. 3C). Counts of immunogold-labeled citrullinated proteins also supported the morphologic observations (Fig. 4I). These results indicate that citrullinated proteins are significantly increased in various subcellular compartments of hippocampal astrocytes and neurons of scrapie-infected versus control brains.

DISCUSSION

Here, we performed subcellular fractionation and electron microscopic analysis to investigate expression levels and localization patterns of PAD2 and citrullinated proteins in the brains of control and scrapie-infected mice. Unexpectedly, PAD2 protein was found in nuclei of hippocampal astrocytes and neurons; its nuclear expression was significantly greater in scrapie-infected mice versus controls. Unlike PAD4, PAD2 does not contain a nuclear localization signal sequence and it was assumed that only PAD4 is localized in the nucleus, as shown by Nakashima et al (31) in granulocytes, neutrophils, and eosinophils. Studies of nuclear functions of PAD have focused on the PAD4 isotype (12, 13, 32), and PAD2 nuclear localization has not been previously demonstrated. As shown by both subcellular fractionation and immunogold electron microscopy, this is the first report of the nuclear localization of PAD2.

Recently, PAD2 with MBP in myelin was detected in MS white matter using immunogold labeling (30). We found that PAD2 was widely localized in many cellular compartments in astrocytes and neurons in both control and scrapie-infected mice. In addition, we found PAD2 in glial filaments only in astrocytes of scrapie-infected mice. Intermediate filaments in astrocytes are primarily composed of glial fibrillary acidic protein (GFAP), which is extensively citrullinated in the brains of scrapie-infected mice and patients with sporadic Creutzfeldt-Jakob disease (1, 2). We also found that immunogold-labeled citrullinated proteins were associated with glial filaments (Fig. 4), thus characterizing the relationship between PAD2 and its substrates. Peptidylarginine deiminase 2 was also expressed in nuclear fractions at levels similar to those in

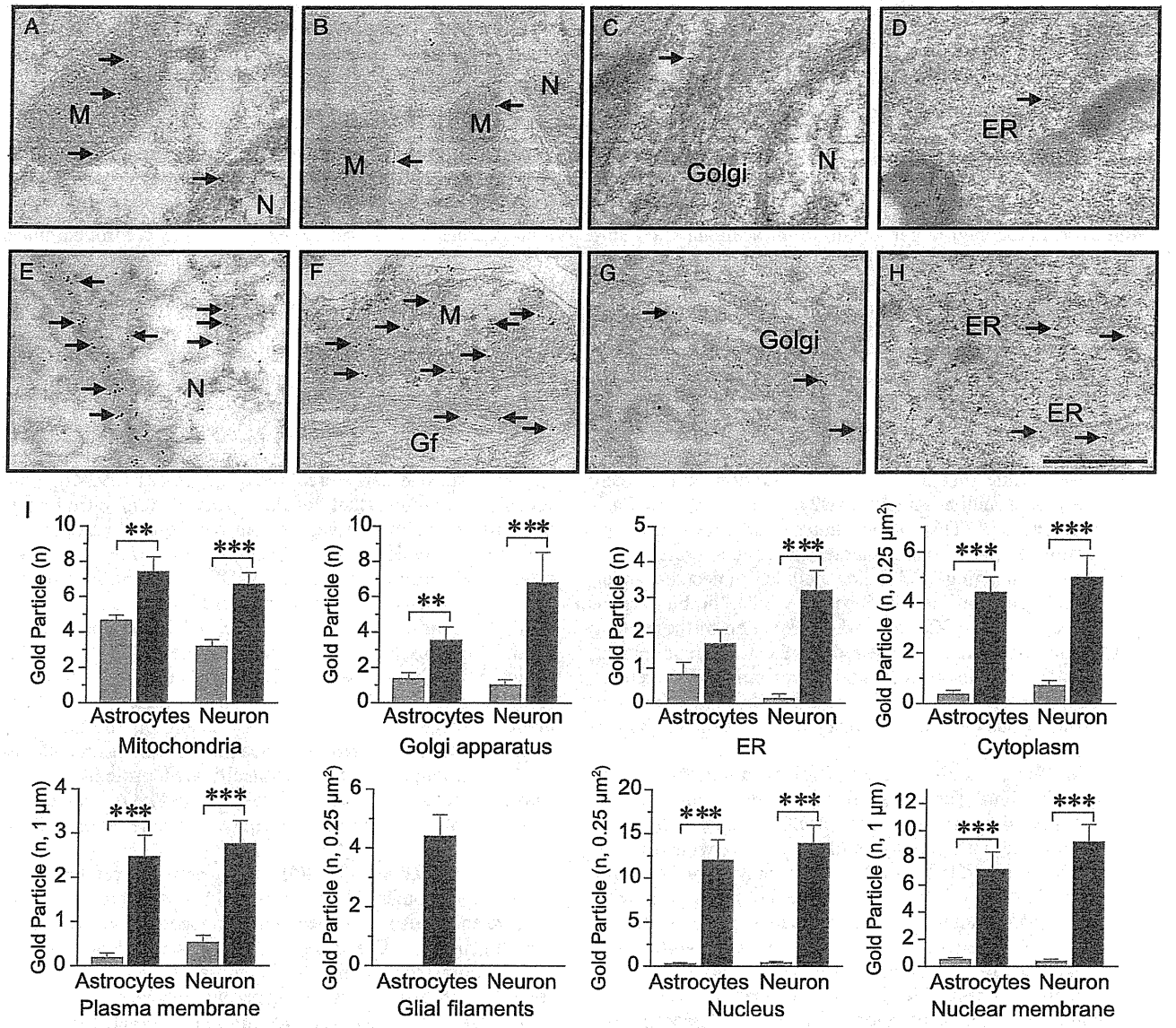

FIGURE 4. Immunogold labeling of citrullinated proteins in hippocampal astrocytes and neurons in control and scrapie-infected brains. **(A–H)** Ten-nanometer immunogold particles (arrows) indicate citrullinated proteins in astrocytes **(A, B, E, F)** and neurons **(C, D, G, H)** of control **(A–D)** and scrapie-infected **(E–H)** brains. ER indicates endoplasmic reticulum; Gf, glial filaments; M, mitochondrion; N, nucleus. Scale bars = 500 nm. **(I)** Immunogold particles of citrullinated proteins were counted in whole mitochondria (n = 31, 28, 30, and 27: respective columns), Golgi apparatus (n = 23, 17, 20, 15), and ER (n = 17, 13, 15, 15). Particles in cytoplasm (n = 19, 20, 21, 18), glial filaments (n = 17), and nucleus (n = 18, 18, 17, 17) were counted in 0.25-μm^2 squares; particles in plasma membranes (n = 16, 14, 19, 16) and nuclear membranes (n = 16, 15, 21, 17) were counted in 1-μm lengths of the membranes. The columns represent the average number of particles at least 13 to 30 different cells in the sections from each sample (control and scrapie-infected, n = 3). Gray columns, control; dark columns, scrapie-infected. Citrullinated proteins were only labeled in glial filaments in astrocytes of scrapie-infected mice. Significant differences in control versus infected: **, $p < 0.01$; ***, $p < 0.001$.

cytosolic expression. By contrast, nuclear PAD4 was hardly detected, and there was no change in its expression level between control and scrapie-infected mice. In our previous report, PAD4 was not detected in the cerebral cortex of patients with sporadic Creutzfeldt-Jakob disease (2). It is unknown whether the active form of PADs in the nucleus is PAD2 and/or PAD4 in the brains of scrapie-infected mice. Our findings indicate that it would be important to determine whether PAD2 is a major factor in the production of citrullinated nuclear proteins or if most of the citrullination is done by PAD4.

The subcellular fractionation data showed that PAD2 was at higher levels in cytosol than in microsomal and mitochondrial fractions. Therefore, the finding of a large number of citrullinated protein bands (some with intense staining in membrane-containing microsomal and mitochondrial fractions [Fig. 1]) was surprising. This may be caused by Ca^{2+} flow between various membrane-containing organelles and plasma membrane. Cytoplasmic Ca^{2+} concentration is mainly modulated by ER and plasma membrane Ca^{2+} channels. Moreover, mitochondria participate in intracellular Ca^{2+} signaling with the ER (33, 34). These cellular compartments are frequently involved in Ca^{2+} mobilization. Thus, Ca^{2+}-related cellular compartments, including ER, mitochondria, and plasma membranes, may facilitate the reaction between PAD enzymes and their substrates.

Previously, it was reported that a significant amount of PAD of unconfirmed type is tightly associated with insoluble membranes in normal mouse cerebral tissues (35). Membrane-bound PAD participates in the destabilization of myelin structure in MS white matter (36, 37). In addition, it has been known that phospholipids allow PAD2 activation in a low Ca^{2+} concentration (38). This demonstrates that PAD2 can actively citrullinate intermediate filament-associated proteins and membranes containing or binding cellular molecules under some unbalanced Ca^{2+} levels. In other words, the binding of lipid molecules to PAD2, and/or the interaction of the protein with cellular membranes, may reduce the Ca^{2+} requirement to physiologically more relevant concentrations. Therefore, membrane-located PAD2 might more rapidly and efficiently citrullinate various intermediate filament and membrane-bound proteins.

We used an anti–modified citrulline antibody for immunogold labeling. The use of this antibody requires chemical modification of protein-bound citrulline residues that then react specifically with peptidylcitrulline but not with free citrulline (27). It is particularly difficult to analyze morphologic changes by electron microscopy because the nickel grids with epoxy-embedded ultrathin sections are damaged by the chemical modification reagents. Nevertheless, we observed immunogold labeling of citrullinated proteins in various cellular compartments, with significantly greater labeling observed in mitochondria, ER, plasma membrane, glial filaments, and nuclear structure of astrocytes and neurons in scrapie-infected versus control mice (Fig. 4). In previous studies, 2-dimensional gel electrophoresis and matrix-assisted laser desorption/ionization-time of flight mass analysis have identified citrullinated candidates, including mitochondrial proteins such as malate dehydrogenase 2 and voltage-dependent anion channel 1; a neuron-specific protein such as NSE; an astrocytes-specific protein such as GFAP; cytoskeletal-associated proteins such as GFAP, MBP, and vimentin; and energy metabolism-associated proteins such as α-enolase, NSE, and aldolase C (1, 2). Therefore, the subcellular distribution of citrullinated proteins labeled by immunogold particles may correlate with these proteomic data (1, 2). We also found remarkable accumulations of citrullinated proteins in the nuclear fraction, suggesting that various nuclear proteins are susceptible to citrullination by PADs during progressive neurodegeneration. It remains to be determined whether increased citrullinated nuclear proteins are caused by nuclear PAD2 or PAD4. Moreover, the factors that facilitate nuclear PAD2 localization need to be identified in future studies.

As in our previous reports, PAD2 was detected not only in reactive astrocytes in brains from prion diseases and AD but also in neuronal cells of the cerebral cortex and Purkinje cells of cerebellum during developmental and aging process (1–3, 28). In the present study, we found PAD2 and accumulated citrullinated proteins in both hippocampal astrocytes and neurons. Thus, PAD2 expression is controlled under appropriate conditions by neuronal and glial cells, and PAD2 may have a role in normal brain development and in neurodegeneration. Although increased intracellular Ca^{2+} levels seem to be the major regulator of PAD2, other factors may be involved in the activation of PAD2 in neuronal and glial cells leading to increase a variety of cell type–specific citrullinated proteins.

In prion diseases, abnormal prion protein (PrP^{Sc}) is a key pathogenic factor that accumulates in lymphoid and neural tissues in early preclinical stages (21, 39, 40). Previously, we found that levels of PAD2 and citrullinated proteins were elevated versus controls from Day 100 to the end stage (Day 150) of ME7 scrapie infection (1). In addition, we determined levels of PAD2 and citrullinated proteins in spleens of scrapie-infected mice. Interestingly, PAD2 was time-dependently decreased in scrapie-infected versus controls, and citrullinated proteins could not be detected (data not shown). This suggests that PrP^{Sc} is not an essential factor for PAD2 activation. Because it is predominantly localized in reactive astrocytes and microglia, PAD2 might be caused by CNS immune responses in prion diseases (1, 2). Although PAD2 and citrullinated proteins are not causative factors in prion diseases, the PAD2 and citrullinated proteins abnormalities may correlate with disease severity.

Accumulation of citrullinated proteins catalyzed by PAD2 or the other PADs is certainly associated with brain damage and is also correlated with proteopathologically related diseases such as AD and prion disease. Accumulation of various citrullinated proteins in membranes might accelerate abnormal cellular responses involving imbalance of cellular metal ion uptake or changes in channel-related proteins. Moreover, as with MBP, increased membrane dissociation and degradation might result. The underlying mechanisms of citrullination of membrane molecules and the clinical implications of the phenomenon remain to be determined.

In summary, we have established the subcellular distribution of PAD2 and citrullinated proteins in control and scrapie-infected mice and showed that levels of both PAD2 and citrullinated proteins were uniformly higher in scrapie-infected brains. Peptidylarginine deiminase 2 is found in various subcellular compartments, including nuclei, but at different concentration levels. We suggest that excessive citrullination may exacerbate destabilization of intracellular compartment organization under pathologic conditions. We hope that our findings will aid in understanding the role of PAD2 and citrullinated proteins in different cellular compartments in brains in normal and neurodegenerative conditions.

REFERENCES

1. Jang B, Kim E, Choi JK, et al. Accumulation of citrullinated proteins by up-regulated peptidylarginine deiminase 2 in brains of scrapie-infected mice: A possible role in pathogenesis. Am J Pathol 2008;173: 1129–42
2. Jang B, Jin JK, Jeon YC, et al. Involvement of peptidylarginine deiminase–mediated post-translational citrullination in pathogenesis of sporadic Creutzfeldt-Jakob disease. Acta Neuropathol 2010;119: 199–210
3. Ishigami A, Ohsawa T, Hiratsuka M, et al. Abnormal accumulation of citrullinated proteins catalyzed by peptidylarginine deiminase in hippocampal extracts from patients with Alzheimer's disease. J Neurosci Res 2005;80:120–28
4. Moscarello MA, Mastronardi FG, Wood DD. The role of citrullinated proteins suggests a novel mechanism in the pathogenesis of multiple sclerosis. Neurochem Res 2007;32:251–56
5. Vossenaar ER, Zendman AJ, van Venrooij WJ, et al. PAD, a growing family of citrullinating enzymes: Genes, features and involvement in disease. Bioessays 2003;25:1106–18
6. Tarcsa E, Marekov LN, Mei G, et al. Protein unfolding by peptidylarginine deiminase. Substrate specificity and structural relationships of the natural substrates trichohyalin and filaggrin. J Biol Chem 1996;271: 30709–16
7. Pritzker LB, Joshi S, Gowan JJ, et al. Deimination of myelin basic protein. 1. Effect of deimination of arginyl residues of myelin basic protein on its structure and susceptibility to digestion by cathepsin D. Biochemistry 2000;39:5374–81
8. Proost P, Loos T, Mortier A, et al. Citrullination of CXCL8 by peptidylarginine deiminase alters receptor usage, prevents proteolysis, and dampens tissue inflammation. J Exp Med 2008;205:2085–97
9. Struyf S, Noppen S, Loos T, et al. Citrullination of CXCL12 differentially reduces CXCR4 and CXCR7 binding with loss of inflammatory and anti–HIV-1 activity via CXCR4. J Immunol 2009;182:666–74
10. Young DS, Meersman F, Oxley D, et al. Effect of enzymatic deimination on the conformation of recombinant prion protein. Biochim Biophys Acta 2009;1794:1123–33
11. Klareskog L, Rönnelid J, Lundberg K, et al. Immunity to citrullinated proteins in rheumatoid arthritis. Annu Rev Immunol 2008;26:651–75
12. Cuthbert GL, Daujat S, Snowden AW, et al. Histone deimination antagonizes arginine methylation. Cell 2004;118:545–53
13. Wang Y, Wysocka J, Sayegh J, et al. Human PAD4 regulates histone arginine methylation levels via demethylimination. Science 2004;306: 279–83
14. Ishigami A, Asaga H, Ohsawa T, et al. Peptidylarginine deiminase Type I, Type II, Type III and Type IV are expressed in rat epidermis. Biomed Res 2001;22:63–65
15. Arita K, Hashimoto H, Shimizu T, et al. Structural basis for Ca(2+)-induced activation of human PAD4. Nat Struct Mol Biol 2004; 11:777–83
16. Mastronardi FG, Wood DD, Mei J, et al. Increased citrullination of histone H3 in multiple sclerosis brain and animal models of demyelination: A role for tumor necrosis factor–induced peptidylarginine deiminase 4 translocation. J Neurosci 2006;26:11387–96
17. Moscarello MA, Wood DD, Ackerley C, et al. Myelin in multiple sclerosis is developmentally immature. J Clin Invest 1994;94:146–54
18. Bhattacharya SK, Crabb JS, Bonilha VL, et al. Proteomics implicates peptidyl arginine deiminase 2 and optic nerve citrullination in glaucoma pathogenesis. Invest Ophthalmol Vis Sci 2006;47:2508–14
19. Musse AA, Li Z, Ackerley CA, et al. Peptidylarginine deiminase 2 (PAD2) overexpression in transgenic mice leads to myelin loss in the central nervous system. Dis Model Mech 2008;1:229–40
20. Prusiner SB. Prions. Proc Natl Acad Sci U S A 1998;95:13363–83
21. Aguzzi A, Calella AM. Prions: Protein aggregation and infectious diseases. Physiol Rev 2009;89:1105–52
22. Pamplona R, Naudí A, Gavín R, et al. Increased oxidation, glycoxidation lipidoxidation of brain proteins in prion disease. Free Rad Biol Med 2008;45:1159–66
23. Giannopoulos PN, Robertson C, Jodoin J, et al. Phosphorylation of prion protein at serine 43 induces prion protein conformational change. J Neurosci 2009;29:8743–51
24. Xanthopoulos K, Polymenidou M, Bellworthy SJ, et al. Species and strain glycosylation patterns of PrP^{Sc}. PLoS One 2009;4:e5633
25. Moody LR, Herbst AJ, Yoo HS, et al. Comparative prion disease gene expression profiling using the prion disease mimetic, cuprizone. Prion 2009;3:99–109
26. Asuni AA, Perry VH, O'Connor V. Change in tau phosphorylation associated with neurodegeneration in the ME7 model of prion disease. Biochem Soc Trans 2010;38:545–51
27. Senshu T, Sato T, Inoue T, et al. Detection of citrulline residues in deiminated proteins on polyvinylidene difluoride membrane. Anal Biochem 1992;203:94–100
28. Shimada N, Handa S, Uchida Y, et al. Developmental and age-related changes of peptidylarginine deiminase 2 in the mouse brain. J Neurosci Res 2010;88:798–806
29. Watanabe K, Akiyama K, Hikichi K, et al. Combined biochemical and immunochemical comparison of peptidylarginine deiminases present in various tissues. Biochim Biophys Acta 1988;966:375–83
30. Wood DD, Ackerley CA, Brand B, et al. Myelin localization of peptidylarginine deiminases 2 and 4: Comparison of PAD2 and PAD4 activities. Lab Invest 2008;88:354–64
31. Nakashima K, Hagiwara T, Yamada M. Nuclear localization of peptidylarginine deiminase V and histone deimination in granulocytes. J Biol Chem 2002;277:49562–68
32. Li P, Yao H, Zhang Z, et al. Regulation of p53 target gene expression by peptidylarginine deiminase 4. Mol Cell Biol 2008;28:4745–58
33. Pizzo P, Pozzan T. Mitochondria–endoplasmic reticulum choreography: Structure and signaling dynamics. Trends Cell Biol 2007;17:511–17
34. Duchen MR, Verkhratsky A, Muallem S. Mitochondria and calcium in health and disease. Cell Calcium 2008;44:1–5
35. Takahara H, Koyama M, Sukawara K. Subcellular location of peptidylarginine deiminase in the mouse brain. Agric Biol Chem 1987;51: 1471–73
36. Moscarello MA, Pritzker L, Mastronardi FG, et al. Peptidylarginine deiminase: A candidate factor in demyelinating disease. J Neurochem 2002; 81:335–43
37. Mastronardi FG, Moscarello MA. Molecules affecting myelin stability: A novel hypothesis regarding the pathogenesis of multiple sclerosis. J Neurosci Res 2005;80:301–8
38. Musse AA, Polverini E, Raijmakers R, et al. Kinetics of human peptidylarginine deiminase 2 (hPAD2)—Reduction of Ca^{2+} dependence by phospholipids and assessment of proposed inhibition by paclitaxel side chains. Biochem Cell Biol 2008;86:437–47
39. Andréoletti O, Berthon P, Marc D, et al. Early accumulation of PrP(Sc) in gut-associated lymphoid and nervous tissues of susceptible sheep from a Romanov flock with natural scrapie. J Gen Virol 2000;81:3115–26
40. Tatzelt J, Groth DF, Torchia M, et al. Kinetics of prion protein accumulation in the CNS of mice with experimental scrapie. J Neuropathol Exp Neurol 1999;58:1244–49

J Physiol Sci (2011) 61:201–209
DOI 10.1007/s12576-011-0139-x

ORIGINAL PAPER

Control of cerebral cortical blood flow by stimulation of basal forebrain cholinergic areas in mice

Harumi Hotta · Sae Uchida · Fusako Kagitani · Naoki Maruyama

Received: 16 July 2010 / Accepted: 1 March 2011 / Published online: 20 March 2011

Abstract We examined whether activity of the nucleus basalis of Meynert (NBM) regulates regional cerebral cortical blood flow (rCBF) in mice, using laser speckle and laser Doppler flowmetry. In anesthetized mice, unilateral focal stimulation, either electrical or chemical, of the NBM increased rCBF of the ipsilateral cerebral cortex in the frontal, parietal and occipital lobes, independent of changes in systemic blood pressure. Most of vasodilative responses to low intensity stimuli (2 times threshold intensity: 2T) were abolished by atropine (a muscarinic cholinergic blocker), whereas responses to higher intensity stimuli (3T) were abolished by atropine and mecamylamine (a nicotinic cholinergic blocker). Blood flow changes were largest when the tip of the electrode was located within the area containing cholinergic neurons shown by choline acetyltransferase-immunocytochemistry. These results suggest that cholinergic projections from basal forebrain neurons in mice cause vasodilation in the ipsilateral cerebral cortex by a combination of muscarinic and nicotinic mechanisms, as previously found in rats and cats.

Keywords Cerebral blood flow · Cholinergic neural pathways · Basal forebrain · Mouse

Introduction

Regulation of blood flow in the cerebral cortex by intracranial cholinergic nerves originating in the magnocellular nucleus of the basal forebrain [nucleus basalis of Meynert (NBM)] and projecting to the cerebral cortex has been first demonstrated in rats (see reviews in [1, 2]), and later in cats [3]. Properties of the vasodilative response were analyzed in detail in rats, since Biesold et al. [4] originally found it by means of laser Doppler flowmetry. This cholinergic vasodilative system, which operates by increasing extracellular ACh release, relies upon activation of both muscarinic and nicotinic cholinergic receptors in the parenchyma of the cortex. The increase in regional cerebral cortical blood flow (rCBF) elicited by this cholinergic vasodilative system is independent of systemic blood pressure and is not coupled to cortical metabolic rates [1, 2]. Focal stimulation of the unilateral NBM produces rCBF increase in frontal, parietal and occipital cortices ipsilateral to the stimulation site [5–7]. However, in cats, focal stimulation of the NBM increases regional blood flow in a restricted area of cerebral cortex in contrast to rats: focal electrical stimulation of the unilateral basal forebrain increased the rCBF of the ipsilateral primary somatosensory cortex that was increased by stimulation of the contralateral forepaw, without any change in blood pressure [3]. The response was the largest when the tip of the electrode was located within the area known to contain the basal forebrain neurons projecting to the primary somatosensory cortex.

Although similar cholinergic projections exist in the cerebral cortex of mice [8], to date it has not been determined whether they mediate vasodilation. Identification of cholinergic functions in normal mouse forebrain is of particular importance because this species is being used increasingly in studies to investigate the genetic control of normal and abnormal cholinergic system functioning [9–11].

Laser speckle flowmetry is useful to assess non-invasively two-dimensional rCBF in the widespread cortices

H. Hotta (✉) · S. Uchida · F. Kagitani · N. Maruyama
Department of Autonomic Neuroscience,
Tokyo Metropolitan Institute of Gerontology,
35-2 Sakae-cho, Itabashi-ku, Tokyo 173-0015, Japan
e-mail: hhotta@tmig.or.jp

with high temporal and spatial resolution. It has been shown that laser speckle flowmetry can image the spatiotemporal dynamics of rCBF changes all over the cortical surface in mice through an intact skull [12]. It is important to clarify whether activation of the NBM produces an increase in rCBF in widespread cortices (as observed in rats), or a restricted cortical area (as observed in cats). Therefore, in this study, we examined the effects of stimulation of the basal forebrain on rCBF in the frontal, parietal and occipital cortices in mice by making concurrent measurements using laser speckle, in addition to laser Doppler flowmetry.

Materials and methods

Experiments were performed on 18 adult male mice (C57BL/6NCr, 30–40 g). All animal experiments were conducted according to the Guidelines for Animal Experimentation prepared by the Animal Care and Use Committee of Tokyo Metropolitan Institute of Gerontology. General experimental procedures with regard to anesthesia, maintenance of respiration, body temperature and monitoring of systemic arterial blood pressure were similar to those described previously [13]. Animals were anesthetized with urethane (1.4 g/kg, intraperitoneally); additional doses were given subcutaneously or intravenously as required to maintain the plane of anesthesia, which was confirmed by the absence of withdrawal and corneal reflexes. The animals were artificially ventilated (Model SN-480-7; Shinano, Tokyo; or Minivent, Harvard, USA) via a tracheal cannula. Their rectal temperature was monitored and maintained at around 38°C. Systemic blood pressure was monitored via a cannula that was inserted into a femoral artery and connected to a pressure transducer.

Measurements of regional cerebral cortical blood flow

Animals were mounted in the prone position on a stereotaxic instrument (Narishige, Tokyo, Japan). In 9 mice, rCBF in the unilateral parietal cortex was measured by a laser Doppler flowmeter (ALF 21D; Advance, Tokyo) with a 0.8-mm-diameter probe placed on the surface of the parietal bone, cleared of periosteum, at about 2 mm lateral to the bregma.

In 7 mice, rCBF was measured by laser speckle contrast imaging (Moor Instruments, Devon, UK). The skin over the skull was removed, allowing the visualization of rCBF changes through the bone. The surface of the skull was covered with saline. The laser speckle contrast imaging device was then fixed, and the zoom was adjusted to cover the entire dorsal surface of the brain from the most anterior part of the olfactory bulbs to the most posterior aspect of the occipital cortex, as described previously [14]. The viewing field covered about 108 mm^2 (12 × 9 mm) with a matrix of 152 × 113 pixels, giving an approximate resolution of 79 μm per pixel. Video images were displayed at 25 Hz with an exposure time of 4 ms and temporally smoothed with a time constant of 1 s. For later analysis, still images were acquired every 1 s (for electrical stimulation) or 6 s (for chemical stimulation) continuously during individual trials, providing 50 or 100 images over a period of 50 s or 10 min, respectively. The acquired images were then averaged over 5-s or 1-min time bins (5 or 10 images per time bin), leading to 10 averaged images. To quantify temporal rCBF changes (in arbitrary units), time courses were extracted in 6 regions of interest (ROI), including the frontal (AP = +0.5 to +2.0 mm from bregma, L = 0.5–2 mm to the midline according to [15]), parietal (AP = 0 to −1.5 mm, L = 1–2.5 mm), and occipital (AP = −2 to −3.5 mm, L = 1.5–3 mm) cortices bilaterally.

Stimulation of the NBM

An electrode, either monopolar (0.2-mm-diameter varnish-insulated tungsten wire, with an exposed sharp tip of 0.2 mm in length) or coaxial (0.1-mm outer diameter, USK-10; Unique Medical, Tokyo), was inserted into the unilateral NBM, after opening a parietal bone in an area of 1 mm in diameter. A 1-cm bare tungsten wire used as the stimulating "return" for the monopolar electrode was inserted into the temporal muscle. The stimulated area was typically located 0.9–1.0 mm posterior to the bregma, 2.0–2.4 mm lateral to the midline, and 3.5–4.2 mm vertical under the bregma height. Focal electrical stimulation of the NBM was performed by means of a stimulator (SEN-7203; Nihon Kohden, Tokyo) and stimulus isolation unit (SS-202J; Nihon Kohden). DC current (50 μA) was applied for 30–60 s at the end of every experiment to localize the stimulated site.

For chemical stimulation, a small needle (31 gauge) was inserted into the NBM. Through the needle, 5–12.5 nmol of sodium L-glutamate in 10–25 nl (Wako Pure Chemicals, Osaka, Japan) was microinjected for a period of 1 min by means of an infusion pump (KD310 Plus; KD Scientific, USA). The same volume of Evans Blue dye was administered at the end of the experiment to localize the injection site.

Mice were killed by injection of an overdose of pentobarbital. The brains were removed, and histological verification of the tip position of the stimulating electrode was carried out using frozen transverse brain sections, each 30–50 μm thickness. Stimulation sites were identified using a mouse brain atlas [15].

Drugs

Cholinergic receptor antagonists were administered intravenously through a femoral venous catheter. Atropine (atropine sulfate; Sigma, USA) at 10 mg/kg, was administered as a muscarinic cholinergic receptor antagonist. Mecamylamine (mecamylamine hydrochloride; Sigma) at 10–20 mg/kg was used as a nicotinic cholinergic receptor antagonist.

Immunohistochemistry

Two mice without stimulating electrode implants were deeply anesthetized with pentobarbital and perfused transcardially with phosphate-buffered saline (about 20 ml) followed by 4% paraformaldehyde solution (about 50 ml). The brains were removed and post-fixed with the same fixative for 2 h then stored in phosphate-buffered saline over night, at 4°C. Coronal sections of brain were cut at 40 μm using a Vibratome. Two sections about 0.9 mm posterior to the bregma were immunostained in each mouse. After endogenous peroxidase activity was blocked, sections were subsequently incubated with antiserum against choline acetyltransferase (ChAT; 1:1,000, rabbit anti-ChAT polyclonal antibody; Chemicon, USA) for 48–72 h, horseradish peroxidase-conjugated secondary antibody (MAX-PO, Histofine Simple Stain; Nichirei, Japan) for 2 h. The marker enzyme was visualized by incubating sections with diaminobenzidine. In each mouse, a subset of alternate sections was processed with the omission of the primary antiserum as a control immunostain. The immunohistochemical reactions were negative in the control immunostains. Sections were observed under a light microscope equipped with a digital camera.

Statistical analysis

Data are expressed as the mean ± SEM and were analyzed using one-way repeated-measures ANOVA followed by Dunnett's multiple comparison test, or the Kruskal–Wallis test followed by Dunn's multiple comparison test. A p value of <0.05 was considered to be statistically significant.

Results

Spatio-temporal changes in cortical blood flow

Focal electrical stimulation (50 μA, 50 Hz, 10 s) of the NBM produced an increase in rCBF in widespread areas of the cerebral cortex, whereas rCBF in the olfactory bulb was not affected, as shown in laser speckle flow images (Fig. 1c, d). Blood flow changes were obvious in the cortices ipsilateral to the site of stimulation, whereas only marginal, transient increases were seen in the contralateral cortices as shown in blood flow traces (Fig. 1e–k). Among the ipsilateral cortices, a predominant change in rCBF was observed in the frontal and parietal cortices, where rCBF usually started to increase within a few seconds after the onset of stimulation and reached a maximum about 10 s later, and then gradually returned to the prestimulus value taking about 20–30 s after the end of stimulation (Fig. 1h, j). Systemic blood pressure was unchanged (Fig. 1m). The responses of rCBF were reproducible in successive trials on the same animal. Similar results were obtained in all 4 mice tested. In those mice, the maximum increase of rCBF in the ipsilateral frontal, parietal and occipital cortices were 24 ± 3, 30 ± 6 and 10 ± 1%, respectively, when measured at 0–5 s after the end of stimulation (Fig. 2d–f). There were no significant differences in the response of rCBF between the frontal and parietal cortices. However, the response in the frontal or parietal cortex was significantly larger than that in the occipital cortex ($p < 0.05$). The responses in the contralateral side were much smaller than those in the ipsilateral side, in all three cortices (Fig. 2, compare a–c with d–f). Blood pressure was not significantly influenced.

In the case of the response produced by lower intensity stimuli (10–20 μA, 50 Hz, 10 s, $n = 5$ trials in 3 rats), there were no significant differences in the response of rCBF between the three different cortices (the maximum increase of rCBF in the ipsilateral frontal, parietal and occipital cortices measured at 5–10 s after the end of stimulation were 12 ± 1, 13 ± 3 and 9 ± 2%, respectively).

Stimulation of the NBM with a microinjection of L-glutamate (5–12.5 nmol/10–25 nl) for 1 min also produced a significant increase in rCBF in widespread areas of the cerebral cortex ipsilateral to the site of stimulation (Fig. 3d–f). However, rCBF in the contralateral side was not significantly affected (Fig. 3a–c). The responses of rCBF were reproducible in successive trials on the same animal. In an individual mouse, rCBF usually started to increase after the end of injection, and was maximal between 3 and 6 min post-injection, and then gradually returned to prestimulation levels after more than 3 min. The maximum increase of rCBF in the ipsilateral frontal, parietal and occipital cortices in 4 mice were 6 ± 2, 7 ± 2 and 8 ± 3%, respectively, when measured at 5–6 min after the end of injection (Fig. 3d–f). There were no significant differences in the response of rCBF between the three different cortices. Blood pressure was not significantly influenced. The injection of the same volume of vehicle (phosphate-buffered saline) into the NBM did not produce any significant changes in rCBF.

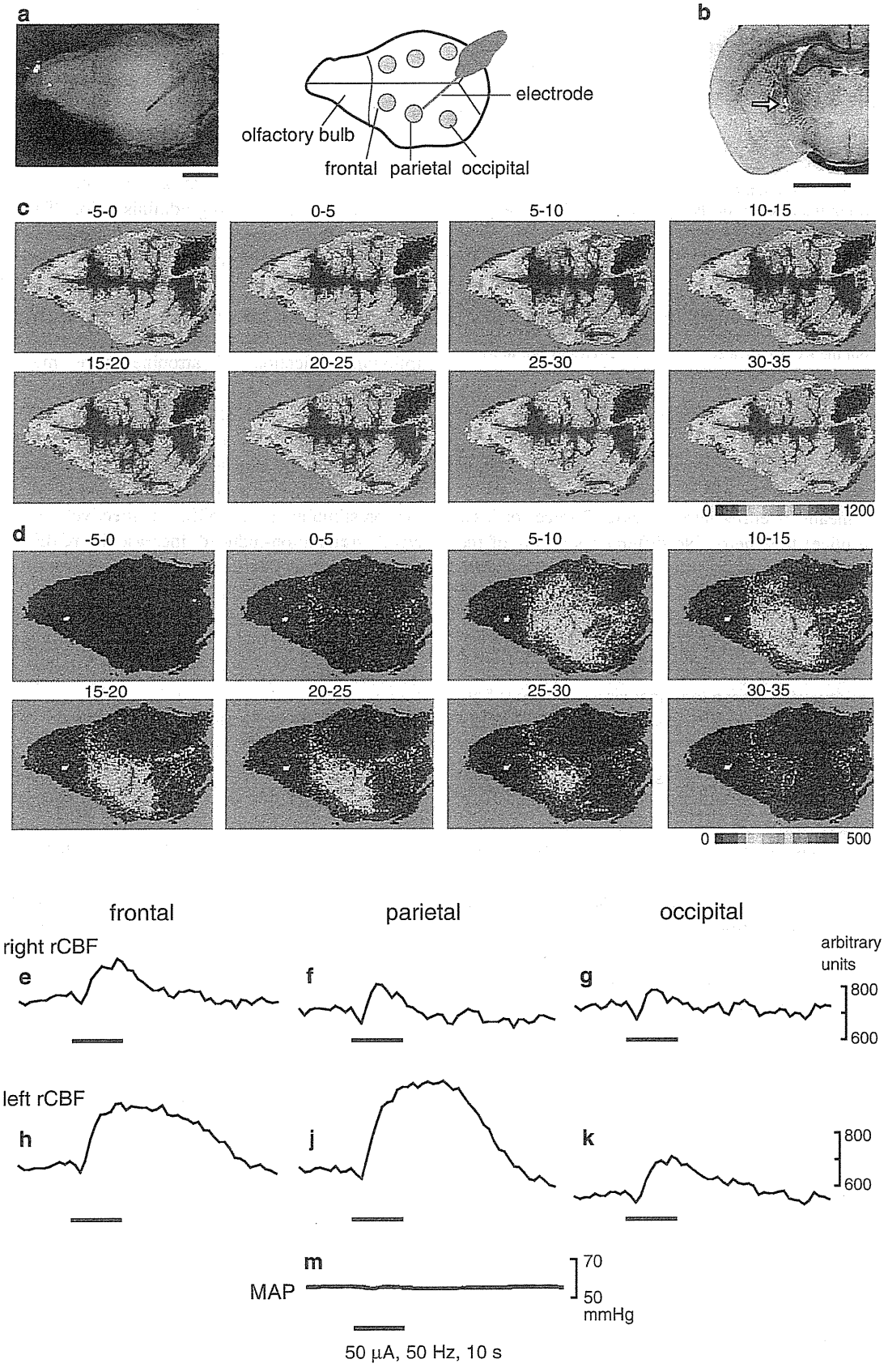
a
b
electrode
olfactory bulb
frontal parietal occipital
c
-5-0
0-5
5-10
10-15
15-20
20-25
25-30
30-35
0
1200
d
-5-0
0-5
5-10
10-15
15-20
20-25
25-30
30-35
0
500
frontal
parietal
occipital
right rCBF
arbitrary units
e
f
g
800
600
left rCBF
h
j
k
800
600
m
MAP
70
50
mmHg
50 μA, 50 Hz, 10 s

◀ **Fig. 1** Spatio-temporal changes in rCBF evoked by focal electrical stimulation of the left NBM in an anesthetized mouse obtained by laser speckle flowmetry. Electrical stimulation of the basal forebrain (0.9 mm posterior to the bregma, 2 mm lateral to the midline, 4 mm vertical under the bregma height, as indicated in (**b**) was carried out at 50 μA, 0.5 ms, 50 Hz, for 10 s. **a** Normal photo image (*left*) and diagram (*right*) of the viewing field, which is the entire dorsal surface of the brain with the olfactory bulb to the left side of each image and the occipital cortex to the right side of each image. **b** Specimen slice of a coronal section of brain on the left side 0.9 mm posterior to the bregma showing the position of the tip of the stimulating electrode (*arrow*). *Scale bars* in (**a**, **b**) represent 2 mm. **c** Averaged flow images over selected periods of 5 s, as indicated above each image (stimulus onset was set as time 0). **d** Differential signal change subtracting the baseline control signal (−5 to 0 s) from subsequent images. rCBF trace in the frontal (**e**, **h**), parietal (**f**, **j**) and occipital (**g**, **k**) cortices contralateral (**e**–**g**) and ipsilateral (**h**, **j**, **k**) to the site of stimulation, extracted from the ROIs indicated by the *gray circles* in (**a**). **m** Mean arterial pressure (*MAP*) simultaneously recorded

Dependence on stimulus parameters

The relations of stimulus current, frequency, and duration to rCBF responses in the parietal cortex were examined in 8 mice, by means of either laser speckle (2 mice) or laser Doppler (6 mice) flowmetry. No differences in any of the measures were found across the two different methods, therefore all data were pooled. When stimulation was applied at a constant frequency of 50 Hz for 10 s (0.5 ms pulse duration), stimulation with currents lower than 10 μA elicited no effect, but stimulation with 25–100 μA produced clear intensity-dependent increases in blood flow (Fig. 4a). Systemic blood pressure was occasionally changed slightly (decreased or increased), but the rCBF response was independent of changes in blood pressure. In half the mice tested, stimulation with 10 μA elicited clear rCBF increase. However, when summarized in 8 mice, significant response was obtained with stimulation above 20 μA (Fig. 4b).

When stimulation was applied at a constant current of 50 μA for 10 s, stimulation at 1–5 Hz elicited no significant effect, but there were frequency-dependent increases in rCBF at 10–100 Hz (Fig. 4c). Responses to 200 Hz stimulation were usually smaller than those to 100 Hz (tested in 6 mice). When the duration of the stimulus train was altered (1–60 s), we found that stimulation with 50 μA at 50 Hz produced a small increase in rCBF by stimulation even when applied for 1 s, and the magnitude of the blood flow changes increased with increasing train durations, reaching its maximum with 10–30 s stimulation (data not shown).

Effects of cholinergic blockers

Repetitive electrical stimulation at 50 Hz was delivered (0.5 ms pulse duration, 10 s stimulus train) at various intensities. We increased the stimulus intensity in 5-μA steps. When rCBF response started to appear in the parietal cortex, the intensity of stimulation was defined as threshold (T). Threshold was between 10 and 25 μA in all 8 mice tested. The maximum increases in cortical rCBF at 2T, 3T and 5T stimulation reached levels that were 23 ± 3, 30 ± 8 and 51 ± 12% above the prestimulus basal rCBF, respectively. We examined the changes in rCBF to NBM stimulation at intensities of 2T, 3T, and 5T before and 20–30 min after each drug administration. The time interval between the administration of drug was usually 50 min. Basal rCBF did not change significantly in response to any drug's administration. The NBM stimulation-induced increase in rCBF was reduced by atropine administration (10 mg/kg, i.v.). The rCBF responses of 2T, 3T and 5T following injection of atropine were much smaller, increasing by 10 ± 3, 22 ± 5 and 38 ± 9% over the prestimulus basal rCBF, respectively (Fig. 5). Residual responses at 2T, 3T and 5T were further reduced by administration of mecamylamine (10–20 mg/kg, i.v.) plus atropine, increasing by 6 ± 2, 10 ± 2 and 18 ± 5% over the prestimulus basal rCBF, respectively (Fig. 5). The NBM stimulation-induced increase in rCBF at 2T was significantly reduced by atropine administration. However, the response at 3T was significantly reduced only after administration of mecamylamine plus atropine. The reduction of rCBF response at 5T was not significant even after administration of mecamylamine plus atropine.

Dependence on stimulated areas

We examined the effect of electrical stimulation (50 μA, 0.5 ms, 50 Hz) for 10 s to various areas at 0.5 mm, 0.9 mm (the usual antero-posterior coordinate) and 1.3 mm posterior to the bregma, and at 0.4-mm increments in the medio-lateral and dorso-ventral axes on blood flow in the parietal cortex in 4 mice. The response of blood flow was the largest when stimulus trains were applied at locations straddling the border between the globus pallidus and the internal capsule, invading both these structures (Fig. 6a). We confirmed the existence of ChAT-immunoreactive neurons at these locations. ChAT-immunoreactive neurons were scattered widely in the basal forebrain, but mainly located in the medial and ventral portion of the globus pallidus and interstitially between the fiber bundles of the internal capsule (Fig. 6b).

Discussion

The basal forebrain contains a population of large cholinergic neurons sending axons to the cerebral cortex in many species [16]. Experiments in rats revealed that stimulation of the NBM produces an increase in rCBF in the cerebral

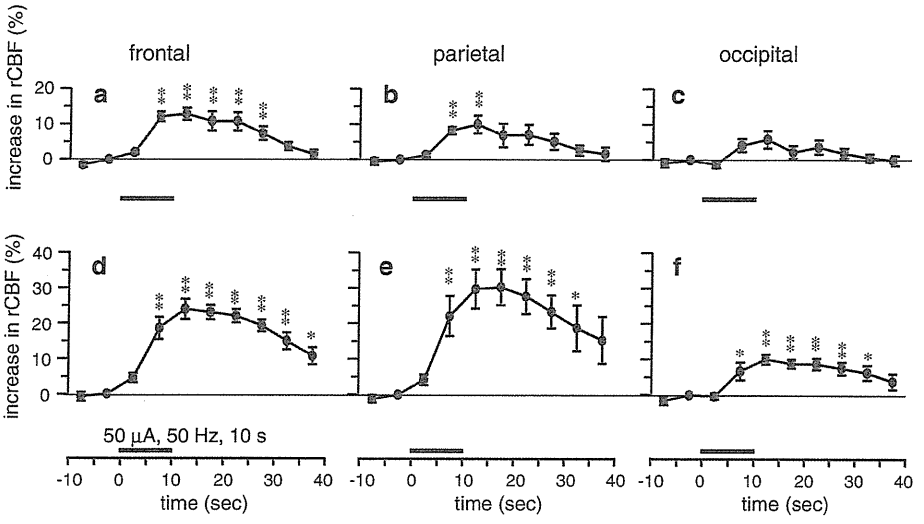

Fig. 2 Summary of the responses of rCBF induced by focal electrical stimulation of the unilateral NBM (50 μA, 0.5 ms, 50 Hz, 10 s) obtained by laser speckle flowmetry. rCBF changes during the 50-s trial averaged every 5 s in the frontal (**a**, **d**), parietal (**b**, **e**) and occipital (**c**, **f**) cortices, contralateral (**a**–**c**) and ipsilateral (**d**–**f**) to the site of stimulation, expressed as the percentage increase from the prestimulus control rCBF ($n = 8$ in 4 mice). $^{*}p < 0.05$, $^{**}p < 0.01$ by one-way repeated-measures ANOVA followed by Dunnett's multiple comparison test

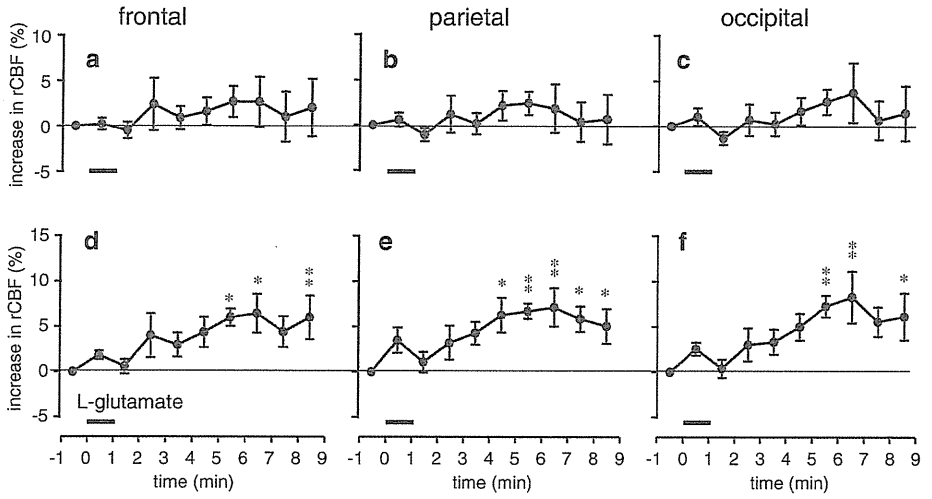

Fig. 3 Summary of the responses of rCBF following microinjection of L-glutamate (5–12.5 nmol/10–25 nl) into the unilateral NBM obtained by laser speckle flowmetry. rCBF changes during the 10-min trial averaged every 1 min in the frontal (**a**, **d**), parietal (**b**, **e**) and occipital (**c**, **f**) cortices, contralateral (**a**–**c**) and ipsilateral (**d**–**f**) to the site of stimulation, expressed as the percentage increase from the prestimulus control rCBF ($n = 7$ in 4 mice). $^{*}p < 0.05$, $^{**}p < 0.01$ by one-way repeated-measures ANOVA followed by Dunnett's multiple comparison test

cortex independent of changes in both systemic blood pressure and regional metabolism [1, 2]. It has been shown using laser Doppler flowmetry [5] and [^{14}C]iodoantipyrine [6, 7] that vasodilation in response to basal forebrain stimulation is produced in the frontal, parietal and occipital cortices. The present results demonstrate with laser speckle flowmetry for the first time that focal stimulation, either electrical or chemical, of the NBM produces an increase in rCBF in mice in widespread cerebral cortical areas, and that these changes are independent of changes in systemic arterial pressure.

In the present study, the rCBF response during stimulation of the NBM was similar to that observed in rats in most aspects, including response magnitude and time course, as well as stimulus strength dependence and frequency dependence of the response, laterality with responses being produced predominantly in the ipsilateral cortex, and contribution of both muscarinic and nicotinic receptors [4]. These findings suggest that the cerebral vasodilation as a result of electrical stimulation of the NBM is attributed mostly to increased release of acetylcholine from the cholinergic projecting systems to the cortex originating in the NBM.

The retrograde transport experiments in rats [17, 18] and cats [19] revealed that basal forebrain projections to the parietal cortex arise from neurons that are scattered widely

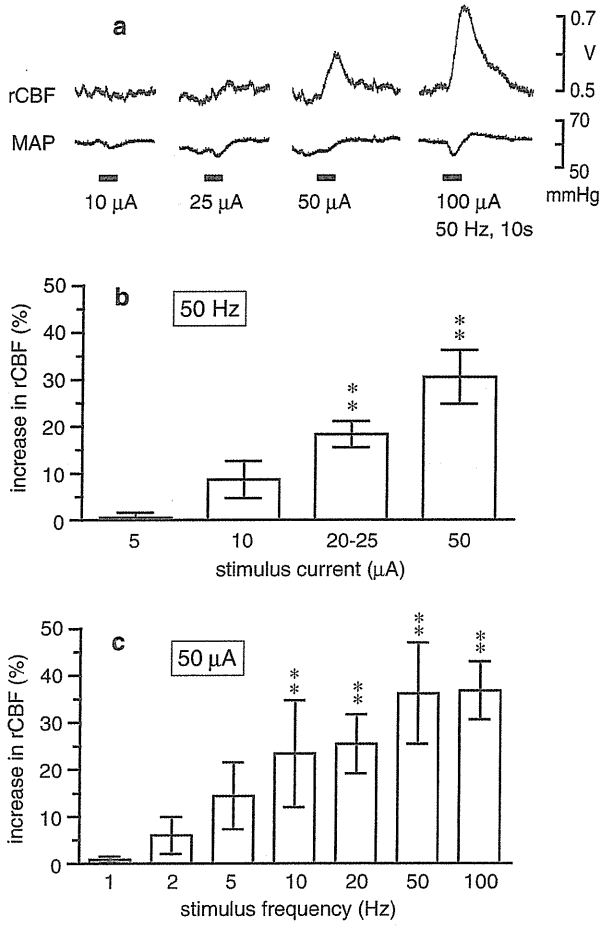

Fig. 4 Changes in rCBF in the parietal cortex ipsilateral to the stimulated NBM. **a** Sample recordings of rCBF obtained by laser Doppler flowmetry and mean arterial pressure (MAP) in a mouse. **b, c** Summarized responses of rCBF measured at maximum level and expressed as the percentage increase from the prestimulus control rCBF. Each *column* and *vertical bar* shows the mean ± SEM ($n = 8$). Data depict blood flow changes measured by laser Doppler ($n = 6$) or laser speckle ($n = 2$) flowmetry. $^{**}p < 0.01$; significantly different from prestimulus control rCBF by one-way repeated-measures ANOVA followed by Dunnett's multiple comparison test

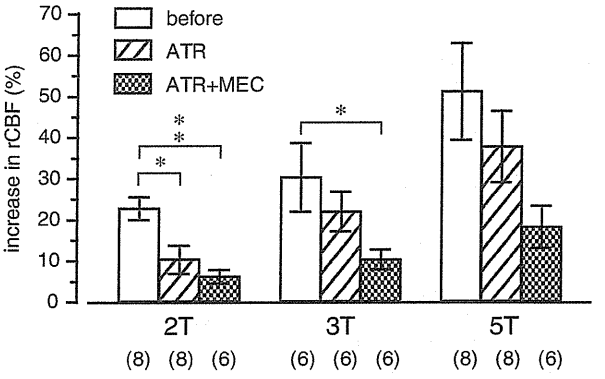

Fig. 5 The effects of muscarinic and nicotinic cholinergic receptor blockers (*ATR* atropine, *MEC* mecamylamine) on the rCBF response in the parietal cortex induced by stimulation of the NBM (0.5 ms, 50 Hz, for 10 s). Summarized responses of rCBF measured at maximum level and expressed as percentage increase from the prestimulus control rCBF ($n = 6$ or 8, shown in *parentheses*). Data depict blood flow changes measured by laser Doppler ($n = 6$) or laser speckle ($n = 2$) flowmetry. $^{*}p < 0.05$, $^{**}p < 0.01$; significantly different from control response before injection of cholinergic receptor blockers by the Kruskal–Wallis test followed by Dunn's multiple comparison test

in the ipsilateral basal forebrain, but mainly located in the medial and ventral portion of the globus pallidus and interstitially between the fiber bundles of the internal capsule. Stimulation in this area produced the largest changes in rCBF in our mice, and blood flow increases were reduced by muscarinic and nicotinic receptor antagonists. Finally, our immunocytochemical experiments confirmed a high density of large neurons containing choline acetyltransferase in this region of the basal forebrain as reported previously in mice [8], suggesting that a significant portion of this projection is cholinergic, resembling reported projections in rats [4, 20, 21]. It is interesting that most of the blood flow change induced by low intensity stimulation was reduced by atropine, but the addition of mecamylamine was necessary to reduce changes caused by larger stimuli. These larger stimuli are likely to activate a greater number of cholinergic (and perhaps non-cholinergic) projection neurons, suggesting that different parts of the projection preferentially target muscarinic or nicotinic elements. This is a complex issue that may well benefit from additional studies in mice that can employ specific genetic mutations to help unravel the cholinergic receptor pharmacology of the cerebral vasculature.

When the rCBF responses in the ipsilateral frontal, parietal and occipital cortices following either electrical or chemical stimulation of the NBM were compared, there were some differences. Firstly, time course of the blood flow responses to glutamate injection was markedly different from those to the electrical stimulation. This result is similar to the previous report in rats that the maximum flow response was sometimes observed 10–20 min after glutamate injection [5]. The reason for slow peak latency following focal glutamate injection may be related to the fact that cholinergic neurons in the NBM are scattered widely in the basal forebrain of rats and mice (see Fig. 6). Focally injected glutamate would diffuse around the site of injection, and then would gradually recruit excitation of many cell bodies of the vasodilator fibers. Secondly, responses to glutamate and lower intensity electrical stimuli showed no significant differences between the sites of the recording, whereas those to higher intensity electrical stimuli were larger in the frontal and parietal cortex than those in the

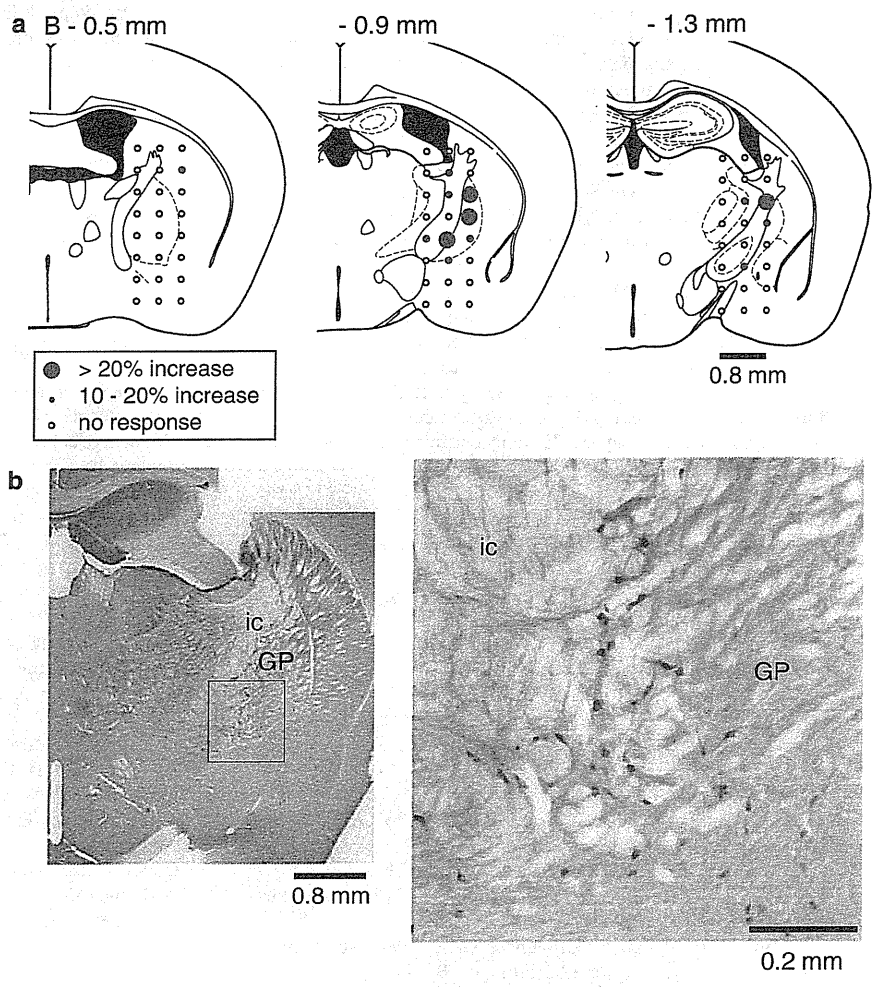

Fig. 6 **a** Diagrams of 3 different coronal sections of mouse brain showing the relationship between stimulating sites and rCBF responses in the parietal cortex with brain electrical stimulation (50 μA, 0.5 ms, 50 Hz, for 10 s). The diagram depicts slices 0.5, 0.9 and 1.3 mm posterior to the bregma, with 24 stimulating sites shown in each slice. *Filled circles* indicate stimulation sites that led to increased rCBF, and the size of *circles* represents the magnitude of the responses. *Open circles* indicate no significant response. All data were summarized from the results of 4 mice. **b** Photomicrographs illustrating ChAT-immunostained neurons in the NBM. *GP* globus pallidus, *ic* internal capsule

occipital cortex. These results indicate that the cell bodies of the vasodilator fibers are located in the site where we had injected glutamate and the tip of the stimulus electrode. The higher intensity stimuli may cause excitation of passing fibers going to the frontal and parietal cortices, in addition to activating neuronal soma. This consideration is well in accord with our results that the response was more sensitive to cholinergic blockers when stimulus intensity was lower.

Blood flow is important for every tissue, especially for the brain that is vulnerable to even transient disturbance of its blood supply. NBM stimulation-induced vasodilatation in parenchymal microvessels results in protection against delayed neuronal death following transient ischemia in the rat's cerebral cortex [22–24]. In mice, nicotine treatment [25] or voluntary exercise [26] reduced amyloid load in transgenic models of Alzheimer's disease. In these studies, however, cerebral blood flow was not measured. Since such pharmacological and physiological stimuli can activate NBM [2, 27], the present increase in rCBF would contribute to the reduction of beta amyloidosis by facilitating clearance of beta-amyloid.

Acknowledgment We thank Ms Chieko Kanai for her help in the immunohistochemical study.

References

1. Sato A, Sato Y (1992) Regulation of regional cerebral blood flow by cholinergic fibers originating in the basal forebrain. Neurosci Res 14:242–274
2. Sato A, Sato Y (1995) Cholinergic neural regulation of regional cerebral blood flow. Alzheimer Dis Assoc Disord 9:28–38
3. Hotta H, Uchida S, Shiba K (2007) Cerebral cortical blood flow response during basal forebrain stimulation in cats. Neuroreport 18:809–812
4. Biesold D, Inanami O, Sato A, Sato Y (1989) Stimulation of the nucleus basalis of Meynert increases cerebral cortical blood flow in rats. Neurosci Lett 98:39–44
5. Adachi T, Biesold D, Inanami O, Sato A (1990) Stimulation of the nucleus basalis of Meynert and substantia innominata produces widespread increases in cerebral blood flow in the frontal, parietal and occipital cortices. Brain Res 514:163–166

6. Adachi T, Inanami O, Ohno K, Sato A (1990) Responses of regional cerebral blood flow following focal electrical stimulation of the nucleus basalis of Meynert and the medial septum using the [^{14}C]iodoantipyrine method in rats. Neurosci Lett 112:263–268
7. Vaucher E, Borredon J, Seylaz J, Lacombe P (1995) Autoradiographic distribution of cerebral blood flow increases elicited by stimulation of the nucleus basalis magnocellularis in the unanesthetized rat. Brain Res 691:57–68
8. Kitt CA, Höhmann C, Coyle JT, Price DL (1994) Cholinergic innervation of mouse forebrain structures. J Comp Neurol 341:117–129
9. Chen KS, Nishimura MC, Armanini MP, Crowley C, Spencer SD, Phillips HS (1997) Disruption of a single allele of the nerve growth factor gene results in atrophy of basal forebrain cholinergic neurons and memory deficits. J Neurosci 17:7288–7296
10. Greferath U, Bennie A, Kourakis A, Bartlett PF, Murphy M, Barrett GL (2000) Enlarged cholinergic forebrain neurons and improved spatial learning in p75 knockout mice. Eur J Neurosci 12:885–893
11. Fragkouli A, Hearn C, Errington M, Cooke S, Grigoriou M, Bliss T, Stylianopoulou F, Pachnis V (2005) Loss of forebrain cholinergic neurons and impairment in spatial learning and memory in LHX7-deficient mice. Eur J Neurosci 21:2923–2938
12. Ayata C, Dunn AK, Gursoy-Ozdemir Y, Huang Z, Boas DA, Moskowitz MA (2004) Laser speckle flowmetry for the study of cerebrovascular physiology in normal and ischemic mouse cortex. J Cereb Blood Flow Metab 24:744–755
13. Engel BT, Sato A, Sato Y (1992) Responses of sympathetic nerves innervating blood vessels in interscapular, brown adipose tissue and skin during cold stimulation in anesthetized C57BL/6J mice. Jpn J Physiol 42:549–559
14. Piché M, Uchida S, Hara S, Aikawa Y, Hotta H (2010) Modulation of somatosensory-evoked cortical blood flow changes by GABAergic inhibition of the nucleus basalis of Meynert in urethane-anaesthetized rats. J Physiol 588:2163–2171
15. Franklin KBJ, Paxinos G (2008) The mouse brain in stereotaxic coordinates. Elsevier, New York
16. Nieuwenhuys R, Voogd J, van Huijzen CHR (1988) The human central nervous system, 3rd edn. Springer, Berlin
17. Bigl V, Woolf NJ, Butcher LL (1982) Cholinergic projections from the basal forebrain to frontal, parietal, temporal, occipital, and cingulate cortices: a combined fluorescent tracer and acetylcholinesterase analysis. Brain Res Bull 8:727–749
18. Baskerville KA, Chang HT, Herron P (1993) Topography of cholinergic afferents from the nucleus basalis of Meynert to representational areas of sensorimotor cortices in the rat. J Comp Neurol 335:552–562
19. Barstad KE, Bear MF (1990) Basal forebrain projections to somatosensory cortex in the cat. J Neurophysiol 64:1223–1232
20. Arneric SP (1989) Basal forebrain neurons modulate cortical cerebral blood flow: increases by nicotinic cholinergic mechanisms. J Cereb Blood Flow Metab 9:S502
21. Lacombe P, Sercombe R, Verrecchia C, Philipson V, MacKenzie ET, Seylaz J (1989) Cortical blood flow increases induced by stimulation of the substantia innominata in the unanesthetized rat. Brain Res 491:1–14
22. Hotta H, Uchida S, Kagitani F (2002) Effects of stimulating the nucleus basalis of Meynert on blood flow and delayed neuronal death following transient ischemia in the rat cerebral cortex. Jpn J Physiol 52:383–393
23. Hotta H, Kanai C, Uchida S, Kanda K (2004) Stimulation of the nucleus basalis of Meynert increases diameter of the parenchymal blood vessels in the rat cerebral cortex. Neurosci Lett 358:103–106
24. Hotta H, Uchida S (2010) Aging of the autonomic nervous system and possible improvements in autonomic activity using somatic afferent stimulation. Geriatr Gerontol Int 10(Suppl 1): S127–S136
25. Nordberg A, Hellström-Lindahl E, Lee M, Johnson M, Mousavi M, Hall R, Perry E, Bednar I, Court J (2002) Chronic nicotine treatment reduces beta-amyloidosis in the brain of a mouse model of Alzheimer's disease (APPsw). J Neurochem 81:655–658
26. Adlard PA, Perreau VM, Pop V, Cotman CW (2005) Voluntary exercise decreases amyloid load in a transgenic model of Alzheimer's disease. J Neurosci 25:4217–4221
27. Uchida S, Hotta H (2009) Cerebral cortical vasodilatation mediated by nicotinic cholinergic receptors: effects of old age and of chronic nicotine exposure. Biol Pharm Bull 32:341–344

British Journal of Nutrition, page 1 of 8

doi:10.1017/S0007114511003643

Bioavailability of vitamin C from mashed potatoes and potato chips after oral administration in healthy Japanese men

Yoshitaka Kondo[1]*, Chihana Higashi[2], Mizuki Iwama[1], Katsuyuki Ishihara[2], Setsuko Handa[1], Hiroyuki Mugita[2], Naoki Maruyama[1], Hidenori Koga[2] and Akihito Ishigami[1]

[1]*Aging Regulation, Tokyo Metropolitan Institute of Gerontology, 35-2 Sakae-cho, Itabashi-ku, Tokyo 173-0015, Japan*
[2]*Research and Development Department, Calbee, Incorporation, 23-6 Kiyohara Kougyoudanchi, Utsunomiya, Tochigi 321-3231, Japan*

(Received 8 March 2011 – Revised 26 May 2011 – Accepted 5 June 2011)

Abstract

Potato (*Solanum tuberosum*) tubers contain vitamin C (VC) and commercial potato chips have more VC content per wet weight by dehydration during frying. However, intestinal absorption of VC from orally ingested potatoes and its transfer to the blood remains questionable. The present study was designed to determine whether the dietary consumption of potatoes affects VC concentration in plasma and urinary excretion of VC in human subjects. After overnight fasting, five healthy Japanese men between 22 and 27 years of age consumed 87 g mashed potatoes and 282 g potato chips. Each portion contained 50 mg of VC, 50 mg VC in mineral water and mineral water. Before and after a single episode of ingestion, blood and urine samples were collected every 30 min or 1 h for 8 h. When measured by subtraction of the initial baseline value before administration of potatoes from the values measured throughout the 8 h test period, plasma VC concentrations increased almost linearly up to 3 h. Subsequently, the values of potato-fed subjects were higher than those of water, but did not differ significantly from those of VC in water ($P=0{\cdot}14$ and $P=0{\cdot}5$). Less VC tended to be excreted in urine during the 8 h test than VC in water alone (17·0 (SEM 7·5) and 25·9 (SEM 8·8) *v.* 47·9 (SEM 17·9) μmol/mmol creatinine). Upon human consumption, mashed potatoes and potato chips provide VC content that is effectively absorbed in the intestine and transferred to the blood. Clearly, potatoes are a readily available source of dietary VC.

Key words: **Bioavailability: Vitamin C: Mashed potatoes: Potato chips**

Potato tubers (*Solanum tuberosum*) are a staple food in many countries worldwide, because they contain an excellent variety of nutrients such as carbohydrates, protein, lipids, dietary fibre, minerals (Zn, Fe, Mg, Ca, K and Na) and vitamins (vitamin C (VC), vitamin B_1, vitamin B_2, vitamin B_6, niacin, pantothenic acid and folic acid)[1,2]. Especially notable is the potato's abundant VC content (35 mg/100 g wet weight)[2]. VC is a potent soluble antioxidant and cofactor for several hydroxylases involved in catecholamine biosynthesis and collagen polymerisation[3]. Since the human body cannot synthesise VC, our VC intake most often comes from foods. Historically, the ingestion of potatoes has contributed to the prevention of VC-deficiency disease, that is, scurvy. Recently, VC has been associated with numerous health benefits including decreased risk of CVD[4], stroke[5–8], age-related cataracts[9,10] and type 2 diabetes mellitus and[11,12] has also decreased the frequency of common colds[13].

Potatoes are usually prepared for eating by baking, boiling, steaming, dehydrating or frying. However, each of these cooking methods causes a lesser or greater loss of VC[1,14,15]. However, we previously found that the VC content per wet weight of commercial potato chips was about twice that of unprocessed raw potatoes[16], because rapid frying and complete dehydration during the frying process minimised VC loss. Similarly, potatoes processed by boiling and mashing retain VC. Thus, mashed potatoes and potato chips seem to be a superior dietary source of VC to promote human health.

The effect of all dietary compounds depends on the retention of nutrients in blood and tissues. Therefore, actual bioavailability represents a fundamental issue. Orally administered VC is first absorbed in the small intestine, delivered to the liver, and then circulates in the blood followed by uptake into various tissues[17–19]. In the kidney, proximal tubules absorb VC in primitive urine and release it into the plasma. When VC concentration in primitive urine exceeds

Abbreviations: AUC, area under the curve; ECD, electrochemical detector; MPA, metaphosphoric acid; VC, vitamin C.

***Corresponding author:** Dr Y. Kondo, fax +81 3 3579 4776, email kondo@tmig.or.jp

NS British Journal of Nutrition

British Journal of Nutrition

the reabsorption capacity in proximal tubules, excess VC is excreted in urine. The bioavailability of VC ingested in water is well understood in human subjects[20–24]. Surprisingly, though, no studies have documented the bioavailability of VC from potatoes prepared by mashing or frying as chips. Therefore, we measured VC concentrations in the plasma and urine of human subjects for 8 h after orally administering mashed potatoes and potato chips.

Subjects and methods

Subjects

A total of five healthy male volunteers aged 22–27 years (24 (SEM 1) years) were enrolled in the present study. Their mean BMI was 20·3 (SEM 2·8) kg/m^2 and did not change significantly during the present study. These subjects took no dietary supplements or medications, did not smoke and were not habitual drinkers of alcoholic beverages. None of the subjects had a chronic illness or food allergy. All study participants were in good health on the basis of a medical history, a physical examination and normal results on clinical laboratory tests, including measurement of total protein (75 (SEM 6) g/l), albumin (57·5 (SEM 4·8) g/l), glucose (4·8 (SEM 0·2) mmol/l), aspartate aminotransferase (15 (SEM 2) U/l), alanine aminotransferase (15 (SEM 6) U/l), TAG (0·26 (SEM 0·12) mmol/l), total cholesterol (4·18 (SEM 0·61) mmol/l), urea N (1·94 (SEM 0·31) mmol/l) and creatinine (72 (SEM 5) μmol/l). The present study was conducted according to the guidelines laid down in the Declaration of Helsinki and all procedures involving human subjects were approved by the Clinical Research Ethics Committee of the Tokyo Metropolitan Institute of Gerontology, Tokyo, Japan. Written informed consent was obtained from all subjects.

Study design

A cross-over study at 4-week intervals was conducted as illustrated in Fig. 1. Subjects enrolled in the study received a 'standard' daily meal during the 3 d before the day of VC testing. The standard menu was as follows: (1) breakfast, consisting of bread, cheese and milk; (2) lunch of a commercial frozen meal (Nichirei Foods Direct, Inc., Tokyo, Japan) and rice (Sato Foods Industries Company Limited, Niigata, Japan); (3) dinner of a commercial frozen meal, rice and miso soup with pork and vegetables (Hanamaruki Foods, Inc., Tokyo, Japan). The standard meal was controlled for the content of VC and other nutrients (Table 1). The amounts of energy, protein, fat, carbohydrates and VC delivered were calculated by using the values provided by the manufacturers and listed in the Standard Tables of Food Composition in Japan[2]. VC concentration in these standard meals, in part, was measured by using HPLC and an electrochemical detector (ECD). For the VC bioavailability study, subjects were fasted >12 h after their last meal. Their urine was thoroughly excreted at 08.00 hours, after which the subjects immediately drank 50 ml mineral water (Coca-Cola (Japan) Company, Limited, Tokyo, Japan). Blood and urine samples were then collected at 09.00 hours, followed by the subjects' ingestion of a test sample consisting of 282 g mashed potatoes including 50 mg VC and 100 ml mineral water (food group 1), 87 g potato chips including 50 mg VC and 100 ml mineral water (food group 2), 50 mg VC (DSM Nutrition Japan K.K., Tokyo, Japan) freshly dissolved in 100 ml mineral water (food group 3) and 100 ml mineral water (food group 4) at 4-week intervals. Their blood was then sampled every 30 min for up to 4 h and every 1 h from 4 to 8 h. Urine was sampled every 1 h up to 8 h. To provide enough urine samples, the subjects drank 50 ml of mineral water every 1 h until 8 h after collection of the final plasma and urine samples.

Collection of blood and urine samples

For plasma VC analysis, each blood sample was drawn into a VENOJECT® collection tube (Terumo Corporation, Tokyo, Japan) containing EDTA-2K as an anticoagulant. For plasma glucose analysis, each VENOJECT® collection tube contained EDTA-2Na and heparin-Na as an anticoagulant and NaF as an inhibitor of glucose degradation. For clinical laboratory

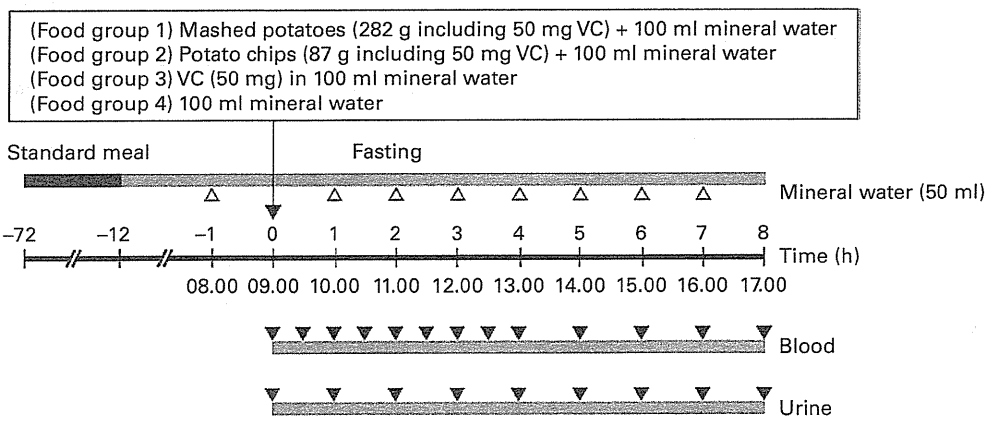

Fig. 1. Scheme of the study in which the same five volunteers were fed at 4-week intervals the following vitamin C (VC) intake: 282 g mashed potatoes containing 50 mg VC with 100 ml mineral water (food group 1), 87 g potato chips containing 50 mg VC with 100 ml mineral water (food group 2), 50 mg VC in 100 ml mineral water (food group 3) and 100 ml mineral water (food group 4). Each food group was orally administered at 08.00 hours on the day of the loading experiment.

Table 1. Composition of the standard meal

	Before the experiments		
	3 d	2 d	1 d
Energy (kJ)	8598	8598	8473
Protein (g)	71·1	67·0	67·4
Fat (g)	57·2	56·0	57·9
Carbohydrates (g)	313·0	319·9	307·5
Vitamin C (mg)	36·3	16·8	13·6

tests of serum, each VENOJECT® collection tube contained procoagulant. Plasma and sera were obtained by centrifugation at 1700 ***g*** for 15 min at 4°C. After plasma was collected, 100 μl of the supernatant were immediately mixed with 450 μl of cold 3% (w/v) metaphosphoric acid (MPA; Wako Pure Chemical Industries Limited, Osaka, Japan) containing 1 mmol/l of the metal ion chelator EDTA (Dojindo Laboratories, Kumamoto, Japan) for VC analysis. Urine samples from each subject were first measured to record their volume; then 600 μl of urine were immediately mixed with an equal volume of cold 10% MPA and 1 mM-EDTA for VC analysis. Remaining aliquots of urine were used for creatinine analysis. All samples were stored at −80°C until use.

Preparation of mashed potatoes and potato chips

Potato (*S. tuberosum* cultivar Toyoshiro) tubers of similar size and appearance were obtained for the experiment from a field in Ibaraki, Japan, in July 2009 and stored for a few days. The unpeeled potatoes were washed in tap water and air-dried on filter paper. In preparation for mashing, potatoes were steamed for 50 min in a steam cooker, peeled, mashed with a potato masher and mixed well with 1% (w/w) salt. The steamed samples were stored at −80°C until use. Potato chips were prepared as the commercial product manufactured by CALBEE, Inc., Tochigi, Japan. That is, peeled potatoes were sliced and immersed in tap water, then fried in rice and palm olein mixing oil for a few minutes. After the frying process, to avoid degradation of VC, potato chips were stored in a N_2 gas-filled pouch with an Al vapour-deposited film at room temperature.

Measurement of vitamin C

VC was measured as the sum of a reduced and oxidised form by using HPLC and ECD as described previously[25]. For analysis of plasma VC, 100 μl of the subjects' plasma were mixed with 450 μl of cold 3% MPA and 1 mM-EDTA and centrifuged at 21 000 ***g*** for 15 min at 4°C. For analysis of VC content in mashed potatoes and potato chips, 0·4 g of samples were homogenised with 14 volumes of cold 5·4% MPA and 1 mM-EDTA by using a high-speed homogeniser (Polytron, Kinematica AG, Lucerne, Switzerland) and centrifuged at 21 000 ***g*** for 15 min at 4°C. For determination of VC after the resulting reduction of an oxidised form to a reduced form, 90 μl of the supernatant were incubated with 10 μl of 350 mM-Tris(2-carboxyethyl)phosphine hydrochloride for 2 h at 4°C. Then, the samples were diluted with 965 μl of cold 5% MPA and 1 mM-EDTA followed by centrifugation at 21 000 ***g*** for 10 min at 4°C. A volume of 10 μl of that supernatant was injected into a Waters 2695 separation module coupled with a Waters 2465 ECD (Nihon Waters K.K., Tokyo, Japan) and separated by using an Atlantis dC18 5 μm column (4·6 × 150 mm; Nihon Waters K.K.) combined with an Atlantis dC18 5 μm guard column (4·6 × 20 mm; Nihon Waters K.K.). The mobile phases consisted of 50 mM-phosphate buffer (pH 2·8), 0·54 mM-EDTA, and 2% methanol. The flow rate was 1·3 ml/min, and temperatures for column and ECD were set at 30°C. Electrical signals were detected by using an ECD with a glassy carbon electrode at +0·6 V. All electrochemical signal data from the ECD were recorded by the Waters Empowere2 software (Nihon Waters K.K.).

Measurement of urinary creatinine

The concentration of creatinine in urine was determined enzymatically by using a Creatinine Test Wako Kit (Wako Pure Chemical Industries, Limited, Osaka, Japan) according to the manufacturer's instructions[26].

Statistical analysis

The values are expressed as mean values with their standard errors. The 8 h area under the curve (AUC) of increased plasma VC concentration was calculated using the trapezoidal rule as a summary measure of VC bioavailability. Statistical analyses were performed with KareidaGraph software (Synergy Software, Reading, PA, USA). The significance of differences among the treatment groups and at different time points was determined by repeated-measures ANOVA. Differences between means were further evaluated by the Tukey's honestly significant difference test. Differences were considered significant at $P<0·05$.

Results

When we compared the two preparations of potatoes, the VC content was 2·24-fold higher in potato chips (57·2 (SEM 0·4) mg) than in mashed potatoes (17·7 (SEM 0·1) mg)/100 g weight. The water content of potato chips (1·9 (SEM 0·1) g/100 g) was marginally 2·5% of the value of mashed potatoes (76·7 (SEM 0·02) g/100 g).

To clarify whether VC from mashed potatoes and potato chips is absorbed in the intestine and transferred to the blood after oral consumption, we serially measured the VC concentrations of the subjects' plasma after consumption of 282 g mashed potatoes and 87 g potato chips, both of which contained 50 mg of VC. Subsequently, each subject also received 50 mg VC in water and water as controls. The four groups of food were administered at 4-week intervals. At the initial measurement of baseline plasma VC concentrations among the recipients of each food group, no significant differences ($P=0·3$) were found for mashed potatoes (34·0 (SEM 4·2) μmol/l), potato chips (40·2 (SEM 3·1) μmol/l), VC in water (41·5 (SEM 2·0) μmol/l) and water (37·2 (SEM 2·1) μmol/l). To compare the later changes after oral

NS British Journal of Nutrition